Supporting Information

# Sulphur- and nitrogen-containing porous donor-acceptor polymers as real-time optical and chemical sensors

*Yaroslav S. Kochergin,[†,‖] Yu Noda,[†] Ranjit Kulkarni, [†] Klára Škodáková, [‡] Ján Tarábek, [‡] Johannes Schmidt, [ǂ] and Michael J. Bojdys[†]**

[†]Department of Chemistry, Humboldt-Universität zu Berlin, Brook-Taylor-Str. 2, 12489 Berlin, Germany

[‖]Department of Organic Chemistry, Charles University in Prague, Hlavova 8, 128 00 Prague, Czech Republic

[‡]Institute of Organic Chemistry and Biochemistry of the CAS, Flemingovo nám. 2, 166 10 Prague, Czech Republic

[ǂ]Institute of Chemistry, Technische Universität Berlin, Hardenbergstraße 40, 10623 Berlin, Germany

## Table of contents

## Materials

All air- and moisture-sensitive reactions were carried out under an argon atmosphere using the standard Schlenk technique. All reagents and solvents were used as received without any additional purification steps. Benzo[1,2-b:4,5-b']dithiophene was purchased from VWR. 1,3,5-Trihydroxybenzene, 2-mercaptoehatnol, and 1.6 M *n*-butyllithium solution were purchased from Acros Organics. Naphtho[2,1-b:6,5-b']dithiophene, trifluoromethanesulfonic acid (TFMSA), and 1M trimethyltin chloride solution were purchased from ABCR. Tetrakis(triphenylphosphine)palladium(0) and 2,5-bis(trimethylstannyl)thieno[3,2-b]thiophene were purchased from Sigma-Aldrich. 1,3,5-Trichlorotriazine was purchased from Alfa Aesar. Completion of reactions was determined by TLC using silica gel (Merck 60, F-254) covered aluminum plates and visualized by UV detection. Column chromatography purification was performed using silica gel (0.063–0.2 mm, 100 mesh ASTM) from Acros Organics.

## Characterisation

**NMR spectra** of monomers were recorded on Bruker Advance 400 MHz spectrometer with $CDCl_3$ as internal standard, which was set at δH = 7.26 ppm. **NMR spectra of polymers in solid state** were measured via $^{13}C$ cross polarization magic angle spinning (CP/MAS) with MAS rate of 12.0 kHz using 4 mm diameter zirconia rotors. Contact time was 10 ms and a relaxation delay - 10.0 s. Crystal structure of polymers was characterized *via* powder X-ray diffraction using Bruker AXS D8 Advanced SWAX diffractometer with Cu Kα (λ = 0.15406 nm) as a radiation source.

**Fourier transform infrared (FT IR) spectra** of the materials were recorded with attenuated total reflection (ATR) technique on an AVATAR 370 FT-IR spectrometer from Thermo Nicolet.

**$N_2$ adsorption/desorption measurements** were performed on the Quantachrome Instruments Autosorb 1C, surface area analyser at 77 K. Samples were degassed at 120 °C for 15 h under

vacuum ($10^{-5}$ Bar) before analysis. Brunauer-Emmett-Teller (BET) surface area ($S_{BET}$) was calculated in relative pressure range ($p/p_0$) from 0.05 to 0.35. Pore size distribution was calculated using Barrett-Joyner-Halenda (BJH) pore model.

**The $CO_2$ adsorption** isotherms were measured at 273 K using a Autosorb-iQ2 from Quantachrome equipped with a Quantachrome CryoCooler for temperature regulation.

**Elemental analyses (C, H and N)** were performed using a PE 2400 Series II CHN Analyzer.

**Inductively coupled plasma optical emission spectrometry (ICP-OES)** measurements were performed using the SPECTRO ARCOS optical emission spectrometer (SPECTRO Analytical Instruments, Kleve, Germany) with radial plasma observation. The SPECTRO ARCOS features a Paschen-Runge spectrometer mount; the wavelength range between 130 and 770 nm can be simultaneously analyzed. An air-cooled ICP-generator, based on a free-running 27.12 MHz system, is installed. For sample introduction cyclonic spray chamber and a modified light nebulizer was used. The following ICP operating parameters were applied: generator power 1 450 W, coolant flow 13 L/min, auxiliary flow 0.8 L/min, nebulizer flow 0.75 L/min, sample aspiration rate 2 mL/min. For calibration, commercially available multielement standard solutions (Analytika, Czech Republic) were used. The concentrations of calibrated elements were 0, 0.2, 1.0, 5.0, 10.0 and 20.0 mg/L, respectively. All measurements were performed in 4% $HNO_3$ as a matrix. Sample preparation: To prepare liquid samples for ICP-OES analysis, the solid samples were weighted (approx. 5 mg) on microanalytical balance and combusted by Schöniger method. After combustion the closed Erlenmeyer flask was treated in ultrasonic bath for several minutes. After absorption of combustion products (at least 2 h) 50 μL of 1000 mg/L Y standard solution were added (final concentration 2 mg/L). Afterwards the liquid mixture was transferred from the glass flask in a plastic bottle. The flask was rinsed carefully with demineralized water which was added to the

plastic bottle. The concentration of $HNO_3$ were adjusted to 4% (w/w in final volume). Then the demineralized water was added to plastic bottle to achieve the final volume of 25 mL (weighed). After mixing the solution was filtered and introduced to the spectrometer system.

**Solid State UV/Vis measurements** were carried out on Cary 6000i UV-Vis-NIR spectrometer from Agilent in reflection mode. The samples were prepared by spreading the polymer powder as a thin film between two quartz microscopic slides. Optical bangaps of obtained materials were *determined using Tauc plot based on the following equation:*

$$F(R) = (\alpha h\nu)^{1/n} = C(h\nu - Eg),$$

where F(R)is the reflectance, a – absorption coefficient, h – Plank's constant, v – frequency of electromagnetic resonance, C – proportionality constant, Eg – bandgap energy. For direct energy transitions n = ½, whereas for indirect – n = 2.[1]

**Solid state fluorescence and time correlated single photon counting (TCSPC) measurements** were recorded on Fluorolog FL3-22 fluorometer (Horiba – Jobin Yvon). For excitation in TCSPC, a picosecond pulsed laser head (NanoLED-375L) with 378 nm centre wavelength was used. Life-time fitting was done using a triple-exponential tailfit. The samples were prepared by spreading the polymer powder as a thin film between two quartz microscopic slides. **Luminescence quantum yields** were determined absolutely using the commercial integrating sphere setup Quantaurus-QY C11347-11 from Hamamatsu.

**Thermogravimetry analysis (TGA)** was performed on Setsys Evolution 18 thermal analyser from Setaram under air and nitrogen atmosphere with the heating rate of 10 $^{o}$C/min and maximum temperature of 1000 $^{o}$C.

**X-ray photoelectron spectroscopy (XPS)** measurements were performed using a ThermoScientific K-Alpha$^+$ X-ray Photoelectron Spectrometer. All samples were analysed using a microfocused, monochromated Al K α X-ray source (1486.68 eV; 400 μm spot size). The analyser had a pass energy of 200 eV (survey), and 50 eV (high resolution spectra), respectively. To prevent any localized charge buildup during analysis the K-Alpha$^+$ charge compensation system was employed at all measurements. The samples were mounted on conductive carbon tape the resulting spectra analysed using the Avantage software from ThermoScientific.

**Scanning electron microscopy (SEM)** was made on Nova NanoSEM 450 microscope from FEI. **Energy-dispersive X-ray spectroscopy (EDX)** was measured at 20.00 kV accelerating voltage and 5.0 spot size with an EDAX Metek Octane Pro Detector.

**Transmission Electron Microscope (TEM)** images and **selected area electron diffraction (SAED)** were carried out using a JEM-1011instrument (JEOL), operating at an accelerating voltage of 80 kV with a spherical aberration coefficient: value of 5.6 mm. Images were recorded on VELETA - side-mounted TEM CCD (charge-coupled device) camera with a resolution of 2K x 2K and with an exposure time of one second per frame and an interval of two seconds between the frames.

**Electron paramagnetic resonance (EPR)** spectra were recorded on an EMX-plus spectrometer (Bruker Biospin) operating at X-band, equipped with the high-sensitivity resonator ER 4119 HS-W1, and the variable temperature unit ER4141VT. Acquisition parameters were microwave power of 1 mW, receiver gain of 1×103, modulation frequency of 100 kHz, modulation amplitude of 1 G, sweep width of 1000 G, time constant of 10.24 ms, conversion time of 40.96 ms, 4 scans, and 1024 data points. The temperature was controlled within ±1 K. The samples were loaded into glass

capillaries (100 µL, i.d.=1.2 mm) which were sealed with wax. The capillaries were inserted in standard quartz ESR tubes (i.d.=3 mm).

**Synthetic protocols and procedures**

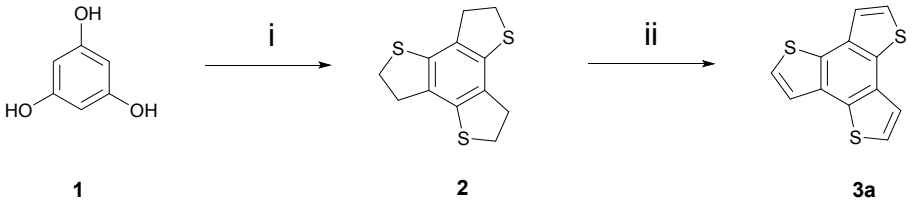


***Scheme S1.*** Synthesis benzotrithiopene BTT (3). i) 2-Mercaptoethanol, TFMSA, chlorobenzene, reflux, 6h; ii) chloranil, toluene, reflux, 2 days;

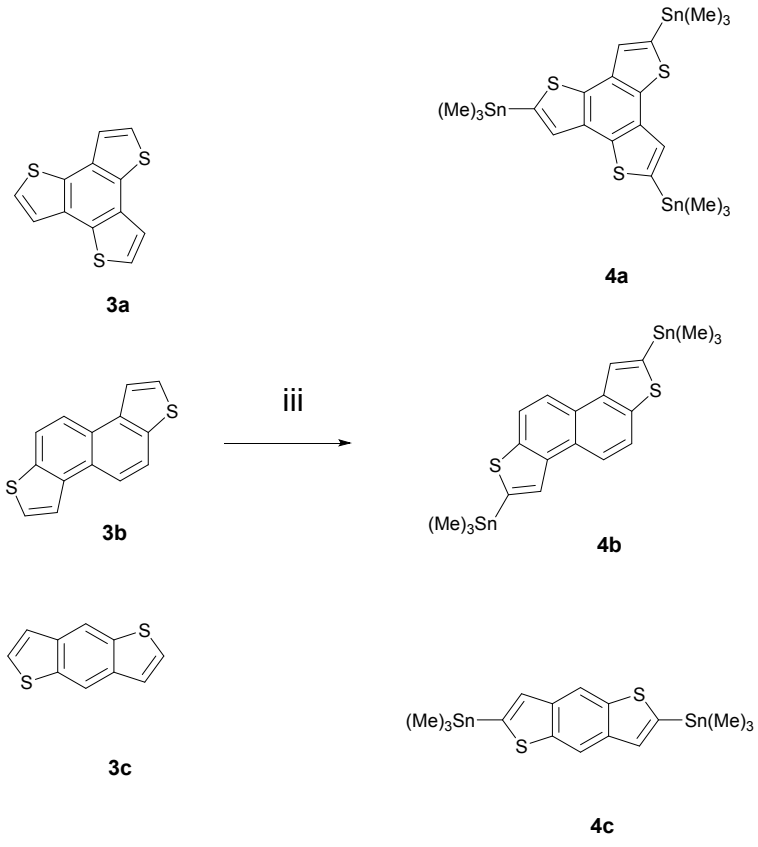


***Scheme S2.*** Synthesis of stannylated derivatives of S-containing monomers. iii) n-BuLi, $Me_3SnCl$, THF.

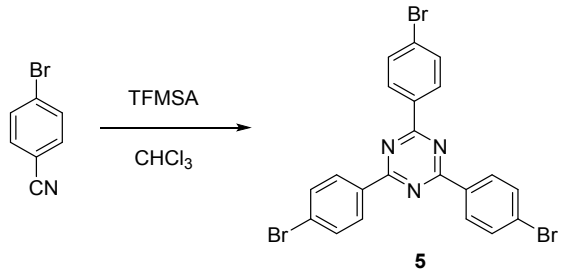


***Scheme S3.*** Synthesis of ,4,6-tris(4-bromophenyl)-1,3,5-triazine.

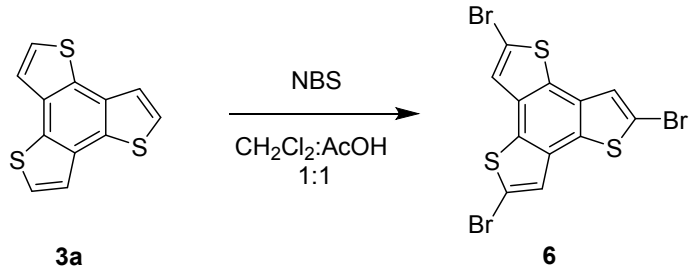


***Scheme S4.*** 2,5,8-Tribromobenzo[1,2-b:3,4-b':5,6-b'']trithiophene.

Compound **(3a)** was synthesized according to modified synthetic protocol, reported by Thongpanchang et. al.[2]

*2,3,5,6,8,9-hexahydrobenzo[1,2-b:3,4-b':5,6-b'']trithiophene* (**2**).

1,3,5-Trihydroxybenzene (**1**) (0.30 g, 2.38 mmol) and 2-mercaptoethanol (1.50 mL, 21.41 mmol) were mixed in dry chlorobenzene (300 mL). TFMSA (1.25 mL, 14.27) was added dropwise under room temperature and the reaction mixture was refluxed than for 6 h. A solid started to appear in the reaction flask during the increase of temperature, but afterwards it was gradually dissolved. The reaction was cooled down to room temperature and neutralized with 5% NaOH (mL). Subsequently the reaction mixture was extracted with $CH_2Cl_2$ (3x mL). Combined extracts were washed with distilled water (3x mL), dried over anhydrous $Na_2SO_4$ and evaporated to dryness. Crude product was purified by silica gel column chromatography using Hexane:$CH_2Cl_2$ 2:1 as an

eluent to provide compound (**2**) as a white solid ( 0.06 g, 10% yield). $^{1}$H NMR (400 MHz, $CDCl_3$, δ/ppm): 3.11 (t, *J* = 7.8 Hz, 6H, $CH_2$), 3.40 (t, *J* = 7.8 Hz, 6H, $CH_2$); $^{13}$C NMR (101 MHz, $CDCl_3$, δ /ppm): 33.6, 33.2, 129.1, 136.3.

*Benzo[1,2-b:3,4-b':5,6-b"]trithiophene* (**3a**).

2,3,5,6,8,9-hexahydrobenzo[1,2-b:3,4-b':5,6-b"]trithiophene (**2**) (0.5 g, 1.98 mmol) and chloranil (2.92 g, 11.88 mmol) were refluxed in toluene (50 mL). Subsequently the reaction mixture was filtered from the excess of chloranil, solvent was evaporated under vacuum, and the crude product was purified by silica gel column chromatography using Hexane:$CH_2Cl_2$ 2:1 as an eluent to afford the desired product **3a** as an off-white solid (0.24 g, 50% yield). ). $^{1}$H NMR (400 MHz, $CDCl_3$, δ/ppm): 7.56 (d, *J* = 5.4 Hz, 3H, Ar-H), 7.66 (d, *J* = 5.4 Hz, 3H, Ar-H); $^{13}$C NMR (101 MHz, $CDCl_3$, δ /ppm): 122.4, 124.9, 131.5, 131.8.

2,5,8-Tris(trimethylstannyl)benzo[1,2-b:3,4-b':5,6-b"]trithiophene (**4a**), 2,7-bis(trimethylstannyl)naphtho[2,1-b:6,5-b']dithiophene (**4b**), and 2,6-Bis-trimethylstannanyl-benzo[1,2-b;4,5-b']dithiophene (**4c**) were synthesized according to reported procedures.[3-5]

*2,5,8-Tris(trimethylstannyl)benzo[1,2-b:3,4-b':5,6-b"]trithiophene* (**4a**).

Benzo[1,2-b:3,4-b':5,6-b"]trithiophene (**3a**) (0.2 g, 0.81 mmol) was dissolved in anhydrous THF (10 mL) under inert atmosphere. The solution was cooled to 0 $^{o}$C using water/ice bath and n-BuLi (3 mL 1,6 M, 4.86 mmol) was added dropwise. The reaction mixture was brought to room temperature and stirred for 6 h. Afterwards, the reaction was again cooled down to 0 $^{o}$C and $M_3SnCl$ (2.67 mL 1M, 2.67 mmol) was added dropwise. Subsequently, the cooling bath was removed, and the reaction mixture was stirred overnight. The reaction was quenched with dist. water (10 ml), extracted with $CH_2Cl_2$ (3x 10 mL), washed with brine (3x 10 mL), and dried over anhydrous

$MgSO_4$. The solvent was removed under reduced pressure, and the crude solid was subjected for recrystallisation from acetonitrile to provide pure product as an off-white powder (0.45 g, 75 % yield). $^1$H NMR (400 MHz, $CDCl_3$, δ/ppm) $^1$H NMR (400 MHz, $CDCl_3$, δ/ppm) 0.57 (s, $J$ = 5.3 Hz, 18H, $CH_3$), 7.72 (s, $J$ = 8.1 Hz, 3H, Ar-H). $^{13}$C NMR (101 MHz, $CDCl_3$, δ /ppm): -8.14, 130.41, 132.73, 135.81, 137.96.

*2,7-bis(trimethylstannyl)naphtho[2,1-b:6,5-b']dithiophene* (**4b**).

Naphtho[2,1-b:6,5-b']dithiophene (**3b**) (0.63 g, 2.62mmol) was dissolved in anhydrous THF (55 mL) under inert atmosphere. The solution was cooled to -78 $^o$C using dry ice/acetone bath and n-BuLi (5.8 mL 1,6 M, 9.28 mmol) was added dropwise. The reaction mixture was stirred at this temperature for 30 min and then 1.5 h at room temperature. The reaction was again cooled down to -78 $^o$C and $M_3SnCl$ (10.5 mL 1M, 10.5 mmol) was added dropwise. After 30 min the cooling bath was removed, and the reaction mixture was stirred overnight at room temperature. The reaction was quenched with dist. water (ml), extracted with $CH_2Cl_2$ (3x55 mL), washed with brine (3x20 mL), and dried over anhydrous $MgSO_4$. The solvent was removed under reduced pressure, and the crude solid was subjected for recrystallisation from acetone to provide pure product as an off-white powder (1.12 g, 75 % yield). $^1$H NMR (400 MHz, $CDCl_3$, δ/ppm) 0.53 (s, 18H, $CH_3$), 8.08 (d, $J$ = 8.7 Hz, 2H, Ar-H), 8.15 (s, 2H, Ar-H), 8.34 (d, $J$ = 8.7 Hz, 2H, Ar-H). $^{13}$C NMR (101 MHz, $CDCl_3$, δ /ppm): -8.12, 120.2, 120.9, 126.1, 130.1, 137.9, 140.1, 141.5.

*2,6-Bis-trimethylstannanyl-benzo[1,2-b;4,5-b']dithiophene (**4c**).*

Benzo[1,2-b:4,5-b']dithiophene (**3c**) (0.63 g, 2.62 mmol) was dissolved in anhydrous THF (55 mL) under inert atmosphere. The solution was cooled to -78 $^o$C using dry ice/acetone bath and n-BuLi (5.8 mL 1,6 M, 9.28 mmol) was added dropwise. The reaction mixture was stirred at this

temperature for 2 h. Subsequently, $Me_3SnCl$ (10.5 mL 1M, 10.5 mmol) was added dropwise. After 30 min the cooling bath was removed, and the reaction mixture was stirred for more 2 h at room temperature. The reaction was quenched with diethyl ether (50 mL), washed with an aqueous sodium bicarbonate, washed with water (3x20 mL), and dried over anhydrous $MgSO_4$. The solvent was removed under reduced pressure, and the crude solid was subjected for recrystallisation from acetonitrile to provide pure product as an off-white powder (1.12 g, 75 % yield). $^1$H NMR (400 MHz, $CDCl_3$): 0.47 (s, 18 H, $CH_3$), 7.45 (s, 2H, Ar-H), 8.30 (s, 2H, Ar-H). $^{13}$C NMR (101 MHz, $CDCl_3$, δ /ppm): -8.33, 115.08, 130.95, 138.59, 141.636, 141.75.

2,4,6-tris(4-bromophenyl)-1,3,5-triazine **(5)** and 2,5,8-Tribromobenzo[1,2-b:3,4-b**'**:5,6-b**''**]trithiophene **(6)** were prepared according to respective reported procedures.[6-7]

**General procedure for Stille-coupling polymerisation**

Overview of all prepared materials could be found in Table S1.

Respective stannylated monomer, brominated monomer and $Pd(PPh_3)_4$ (3:2:5% mol ratio; in case of Benzo[1,2-b:3,4-b':5,6-b"]trithiophene (**3a**) – 1:1:5% mol ratio) were dissolved in anhydrous toluene under inert atmosphere and refluxed for 3 days. In a short time period (1-2 h) the precipitate of polymer started to appear in the reaction flask. After completion of the reaction the precipitate was filtered and washed with hot toluene, DMF, chloroform, THF and methanol (3 times each solvent). Subsequently the Soxhlet extraction was performed using chloroform, THF and methanol (24 h each solvent). Afterwards the solid was dried in the vacuum drying oven at 120 $^o$C for 24 h. More detailed reaction parameters can be found in Table S2.

**Overview of prepared materials**

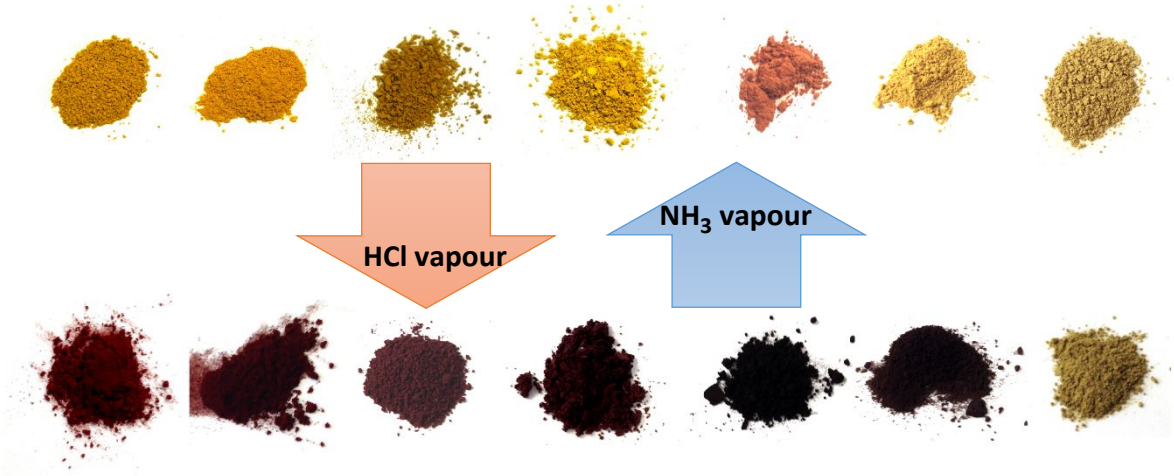


***Figure S1.*** Photographs of prepared materials before (above) and after (below) exposure to HCl vapour. From left to right: **SNP-NDT1, SNP-NDT2, SNP-BTT1, SNP-BTT2, SNP-BDT1, SNP-BDT2, SP-BTT.**

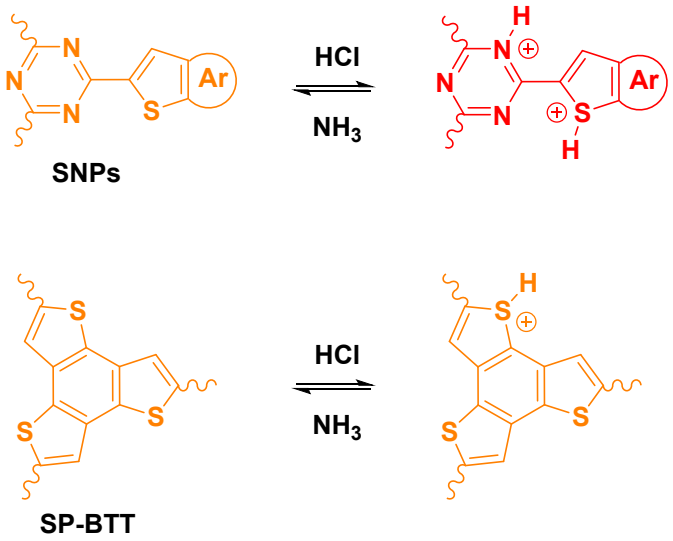


***Scheme S5.*** Suggested protonation pathway of SNPs and SP-BTT (Ar – aryl substituents of the thiophene-containing part of obtained networks).

***Table S1.*** Stille coupling polymerisation conditions.

| Polymer** | Sn-monomer (mmol) | Br-monomer (mmol) | Toluene (mL) | Yield (%) |
|---|---|---|---|---|
| **SNP-BDT1** | 0.96 | 0.65 | 50 | 88.7 |
| **SNP-BDT2** | 0.96 | 0.65 | 60 | 104* |
| **SNP-BTT** | 0.31 | 0.31 | 25 | 68.7 |

*- yield more than 100%for **SNP-BDT2** polymer could be explained by the residue of Pd- and Sn-species, trapped in the polymer matrix, which is proved by elemental analysis and EDX (see results section).

****- Synthetic conditions, as well as EDX, $N_2$ adsorption / desorption, TGA, PXRD, solid-state NMR, SEM and TEM data for SNP-NDT1, SNP-NDT2, SNP-BTT1 and SNP-BTT2 polymers can be found in the manuscript, previously published by us.[8]**

*Solid-state NMR spectra*

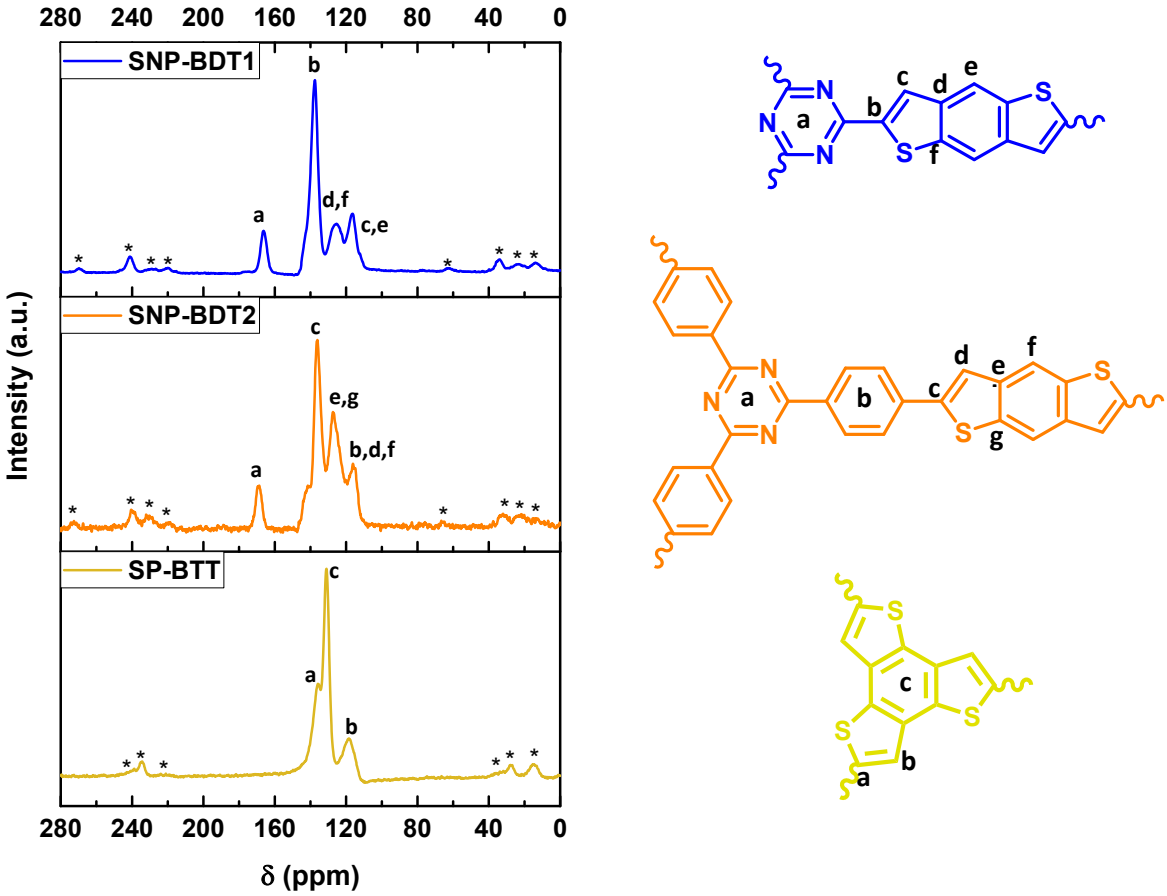


***Figure S2.*** $^{13}$C cross-polarization magic angle spinning solid-state NMR spectra of **SNP-BDT1, SNP-BDT2,** and **SP-BTT**. Spinning side bands are marked with an asterisk (*).

## Nitrogen gas adsorption / desorption analysis

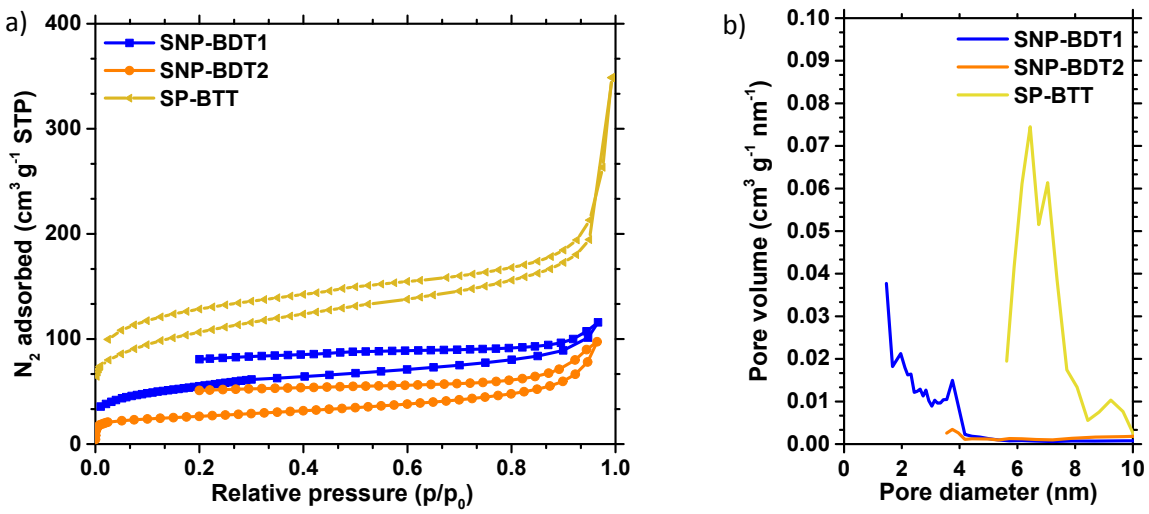


***Figure S3.*** a) $N_2$ ad-/desorption isotherms measured at 77 K and b) pore size distribution plot (PSD) for **SNP-BDT1, SNP-BDT2,** and **SP-BTT.**

## Thermogravimetric analysis (TGA)

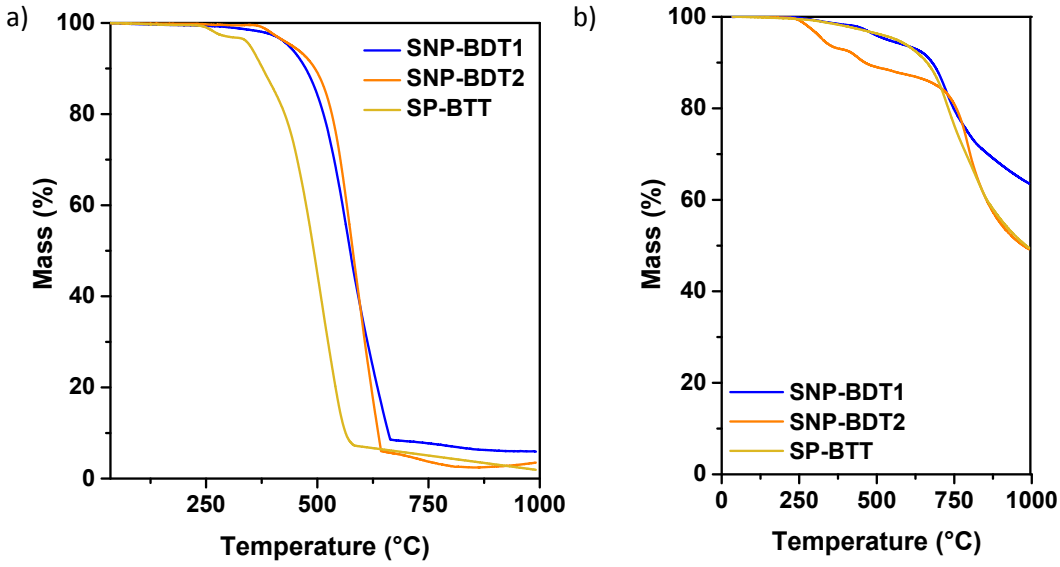


***Figure S4.*** TGA data of **SNP-BDT1, SNP-BDT2,** and **SP-BTT**, heated under air (a) and under $N_2$ (b) atmosphere.

**Powder X-ray diffraction (PXRD).**

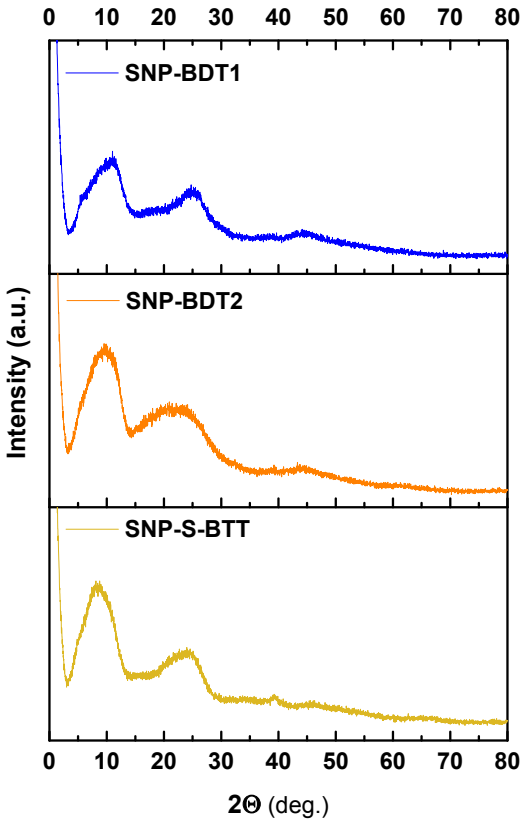


***Figure S5.*** PXRD patterns of **SNP-BDT1, SNP-BDT2,** and **SP-BTT**, measured in the range from 1 to 80 degrees 2θ.

**Scanning electron microscopy (SEM).**

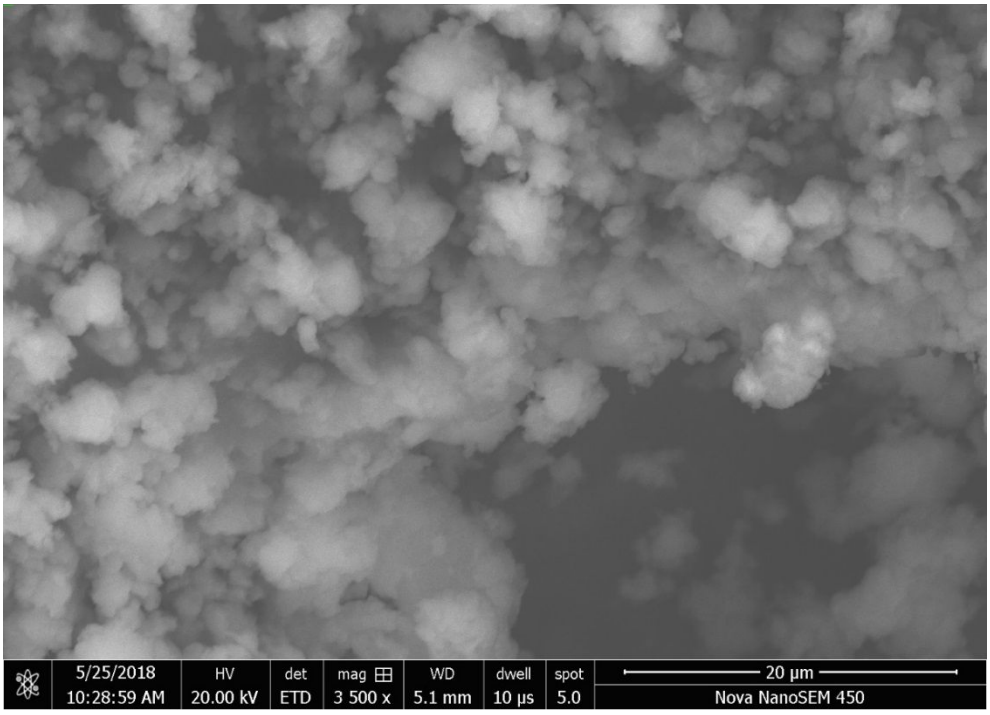


***Figure S6.*** SEM image of **SNP-BDT1.**

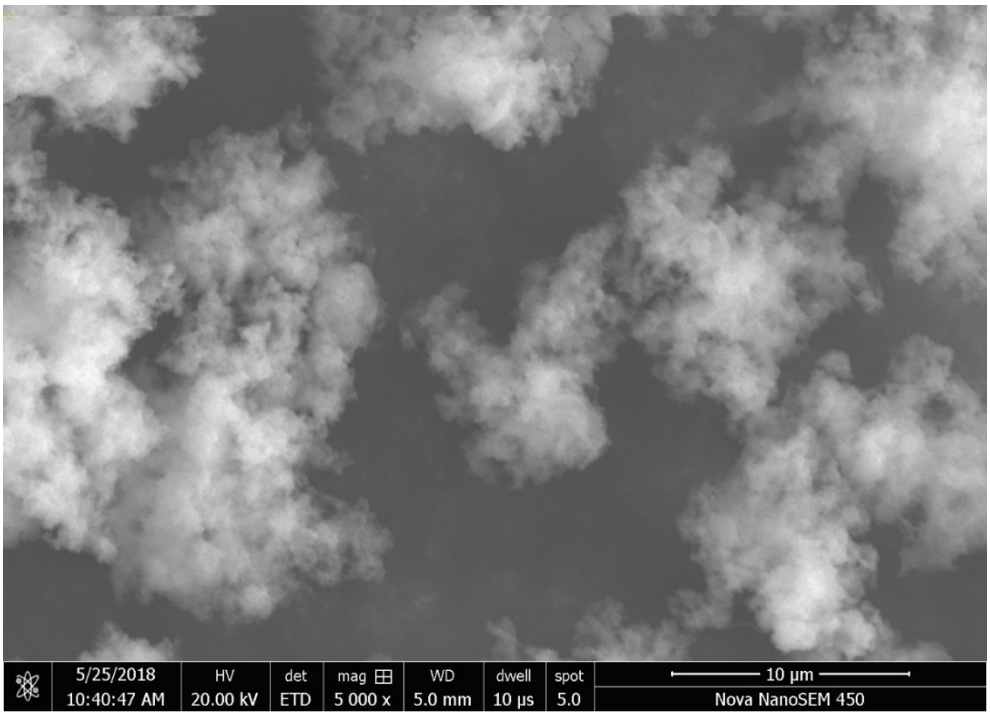


***Figure S7.*** SEM image of **SNP-BDT2.**

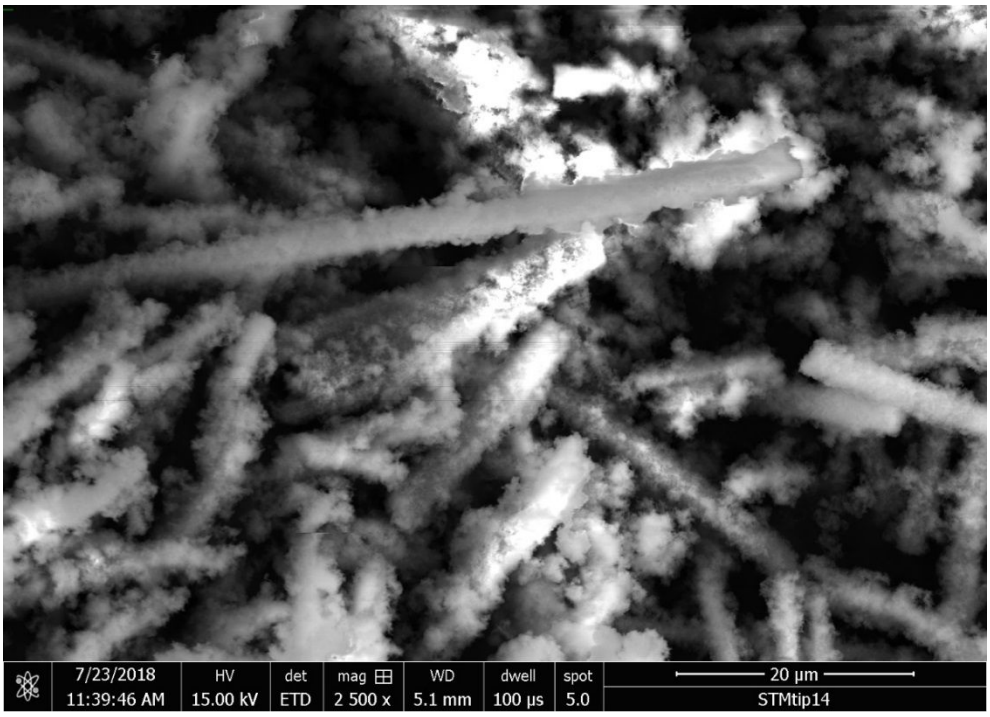


***Figure S8.*** SEM image of **SP-BTT1.**

**Transmission electron microscopy (TEM).**

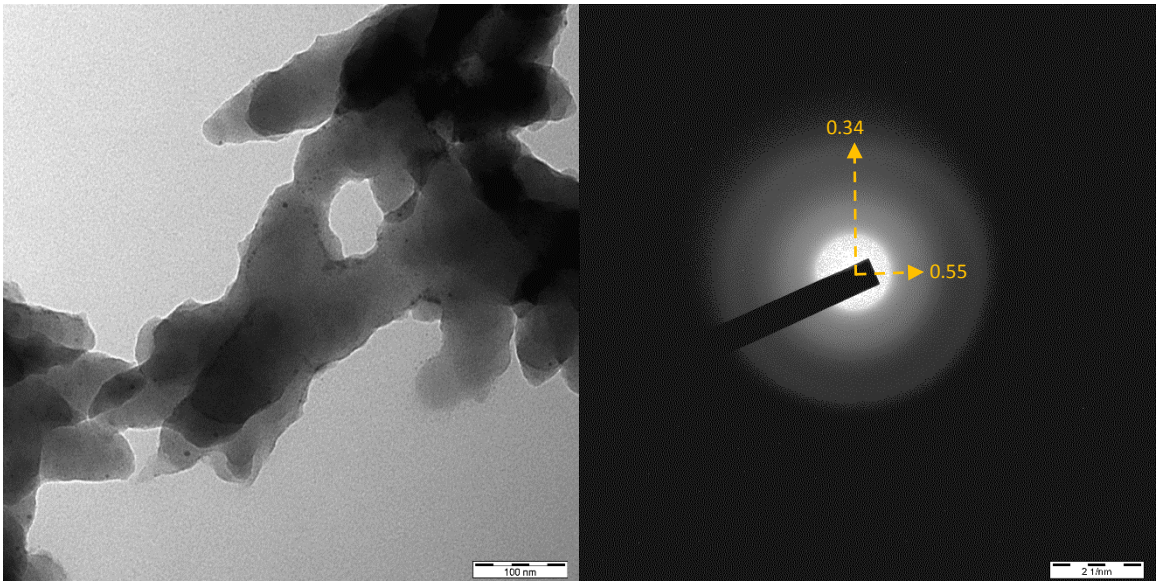


***Figure S9.*** TEM (left) and SAED (right) images with the corresponding ring distances (in nm) of **SNP-BDT1.**

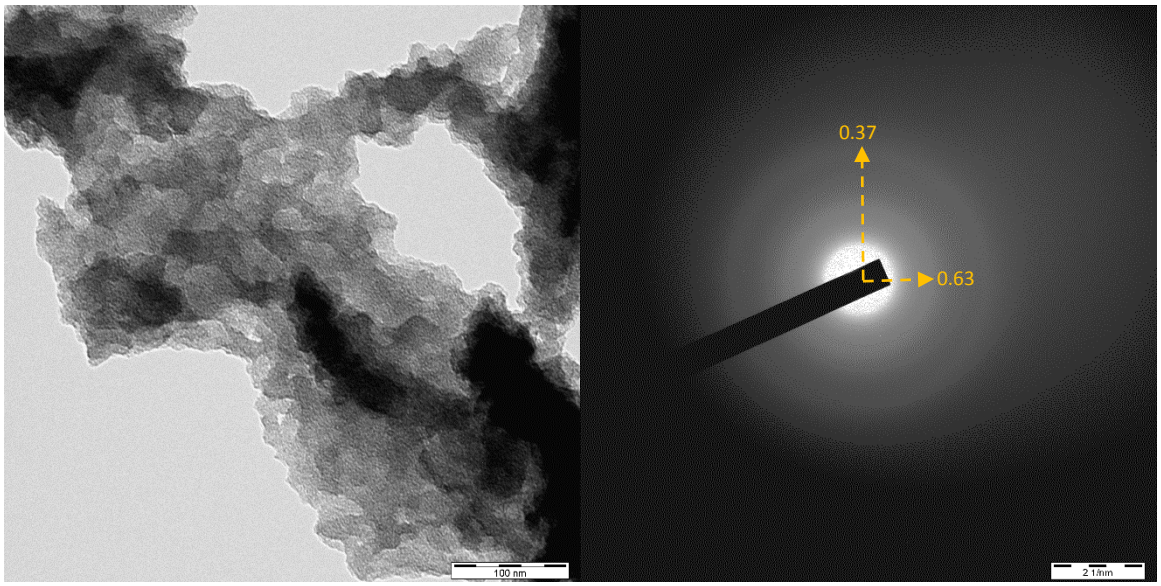


***Figure S10.*** TEM (left) and SAED (right) images with the corresponding ring distances (in nm) of **SNP-BDT2.**

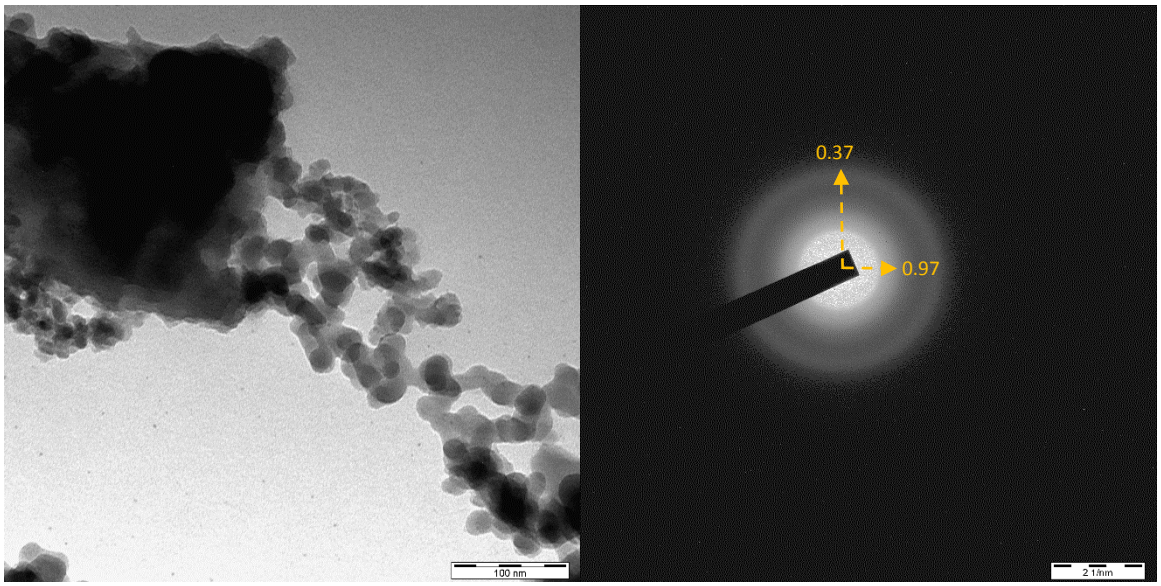


***Figure S11.*** TEM (left) and SAED (right) images with the corresponding ring distances (in nm) of **SP-BTT.**

**Elemental analysis (EA).**

***Table S2.*** EA data (in weight %) for pristine materials.

| Sample | Composition | C (%) | H (%) | N (%) | S (%) | C:N | C:S | Cl (%) | Br (%) | Pd (%) | Sn (%) | P (%) |
|---|---|---|---|---|---|---|---|---|---|---|---|---|
| **SNP-BTT1** | **Theoretical** | 55.02 | 2.77 | 12.83 | 29.37 | 4.3 | 1.9 | 3.72 | n.a. | 0.29 | 0.63 | 0.10 |
| | **Found** | 54.93 | 2.59 | 7.26 | 17.40 | 7.6 | 3.2 | | | | | |
| **SNP-BTT2** | **Theoretical** | 72.11 | 2.75 | 7.64 | 17.50 | 9.4 | 4.1 | 0.94 | 5.74 | 0.12 | 1.03 | 0.36 |
| | **Found** | 62.23 | 2.89 | 5.99 | 13.1 | 10.4 | 4.7 | | | | | |
| **SNP-NDT1** | **Theoretical** | 66.19 | 2.08 | 9.65 | 22.08 | 6.9 | 3.0 | 1.04 | n.a. | 1.05 | 1.15 | 0.16 |
| | **Found** | 51.28 | 2.04 | 8.78 | 22.38 | 5.8 | 2.3 | | | | | |
| **SNP-NDT2** | **Theoretical** | 75.99 | 3.19 | 6.33 | 14.49 | 12.0 | 5.2 | 0.80 | 5.36 | 0.13 | 0.61 | 0.10 |
| | **Found** | 67.77 | 2.98 | 5.05 | 13.07 | 13.4 | 5.2 | | | | | |
| **SNP-BDT1** | **Theoretical** | 59.98 | 1.68 | 11.66 | 26.68 | 5.1 | 2.2 | 1.16 | n.a. | 0.03 | 0.61 | 0.12 |
| | **Found** | 56.01 | 2.11 | 8.93 | 24.16 | 6.3 | 2.3 | | | | | |
| **SNP-BDT2** | **Theoretical** | 73.44 | 3.08 | 7.14 | 16.34 | 10.3 | 4.5 | 0.86 | 2.25 | 0.03 | 0.39 | 0.17 |
| | **Found** | 66.42 | 3.03 | 5.79 | 10.27 | 11.5 | 6.5 | | | | | |
| **SP-BTT** | **Theoretical** | 59.23 | 1.24 | n.a. | 39.53 | n.a. | 1.5 | 0.57 | 5.19 | 0.08 | 1.07 | 0.09 |
| | **Found** | 50.04 | 1.90 | n.a. | 28.97 | n.a. | 1.7 | | | | | |

***Table S3.*** EA data (in weight %) for materials treated with HCl vapours.

| Sample | Composition | C (%) | H (%) | N (%) | S (%) | C:N | C:S | Cl (%) | Br (%) | Pd (%) | Sn (%) | P (%) |
|---|---|---|---|---|---|---|---|---|---|---|---|---|
| **SNP-BTT1** | **Theoretical** | 55.02 | 2.77 | 12.83 | 29.37 | 4.3 | 1.9 | 8.92 | 0.04 | 0.44 | 0.49 | 0.08 |
| | **Found** | 50.58 | 2.55 | 6.58 | 16.52 | 7.7 | 3.1 | | | | | |
| **SNP-BTT2** | **Theoretical** | 72.11 | 2.75 | 7.64 | 17.50 | 9.4 | 4.1 | 9.76 | 5.11 | 0.22 | 0.96 | 0.23 |
| | **Found** | 53.48 | 2.85 | 5.12 | 10.81 | 10.4 | 4.9 | | | | | |
| **SNP-NDT1** | **Theoretical** | 66.19 | 2.08 | 9.65 | 22.08 | 6.9 | 3.0 | 13.28 | n.a. | 1.16 | 0.65 | 0.14 |
| | **Found** | 41.15 | 2.41 | 7.39 | 19.52 | 5.6 | 2.1 | | | | | |
| **SNP-NDT2** | **Theoretical** | 75.99 | 3.19 | 6.33 | 14.49 | 12.0 | 5.2 | 5.86 | 4.33 | 0.16 | 0.62 | 0.09 |
| | **Found** | 62.90 | 2.65 | 4.79 | 11.70 | 13.1 | 5.4 | | | | | |
| **SNP-BDT1** | **Theoretical** | 59.98 | 1.68 | 11.66 | 26.68 | 5.1 | 2.2 | 9.46 | n.a. | 0.78 | 0.53 | 0.08 |
| | **Found** | 49.07 | 2.32 | 7.83 | 19.98 | 6.3 | 2.5 | | | | | |
| **SNP-BDT2** | **Theoretical** | 73.44 | 3.08 | 7.14 | 16.34 | 10.3 | 4.5 | 6.17 | 2.79 | 0.08 | 0.34 | 0.16 |
| | **Found** | 61.33 | 2.85 | 5.52 | 12.90 | 11.1 | 4.8 | | | | | |
| **SP-BTT** | **Theoretical** | 59.23 | 1.24 | n.a. | 39.53 | n.a. | 1.5 | 5.29 | 4.93 | 0.12 | 1.49 | 0.09 |
| | **Found** | 47.70 | 1.68 | n.a. | 28.26 | n.a. | 1.7 | | | | | |

**Energy-dispersive X-ray (EDX) spectroscopy.**

For EDX, the software was forced to show all possible impurities (e.g. Pd, Sn, P, Cl, Br, etc.) in the material.

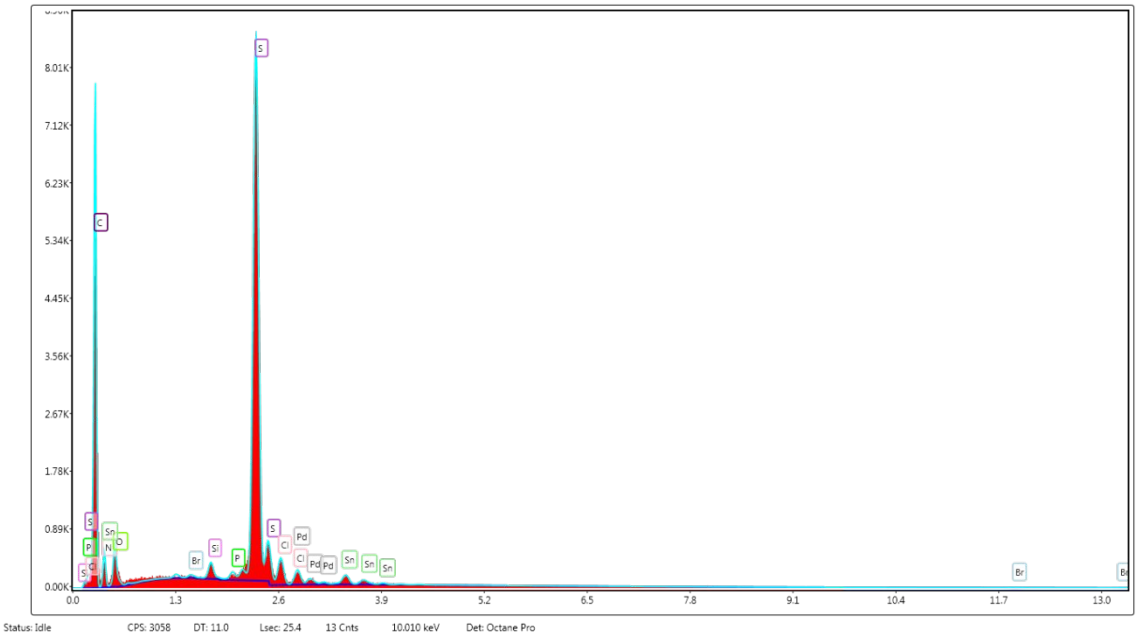


***Figure S12.*** EDX spectra of **SNP-BDT1.**

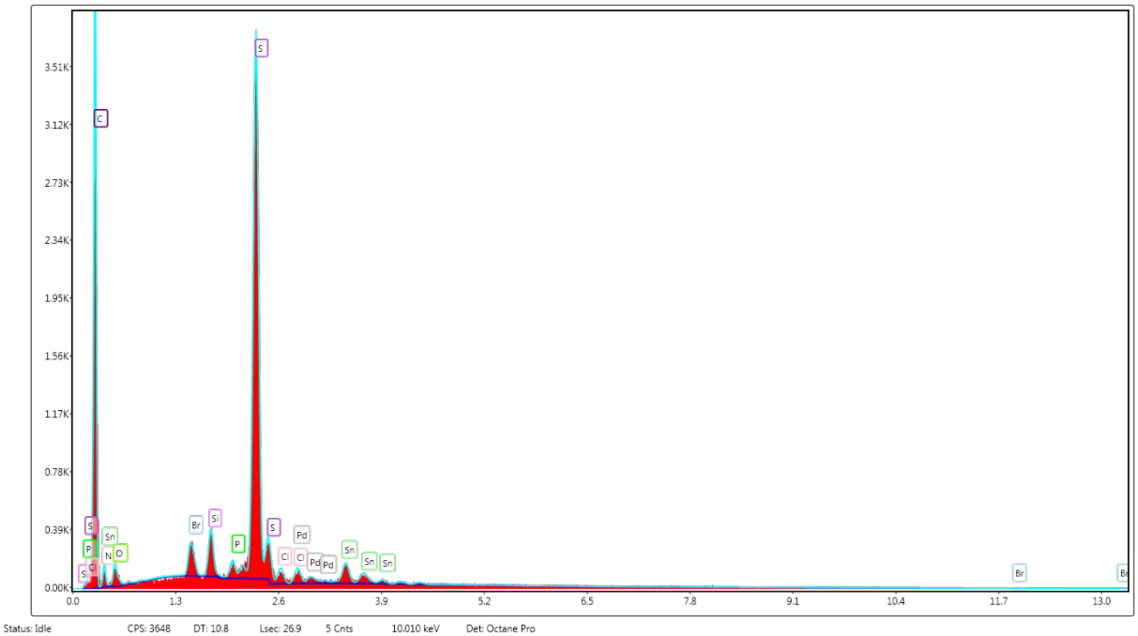


***Figure S13.*** EDX spectra of **SNP-BDT2.**

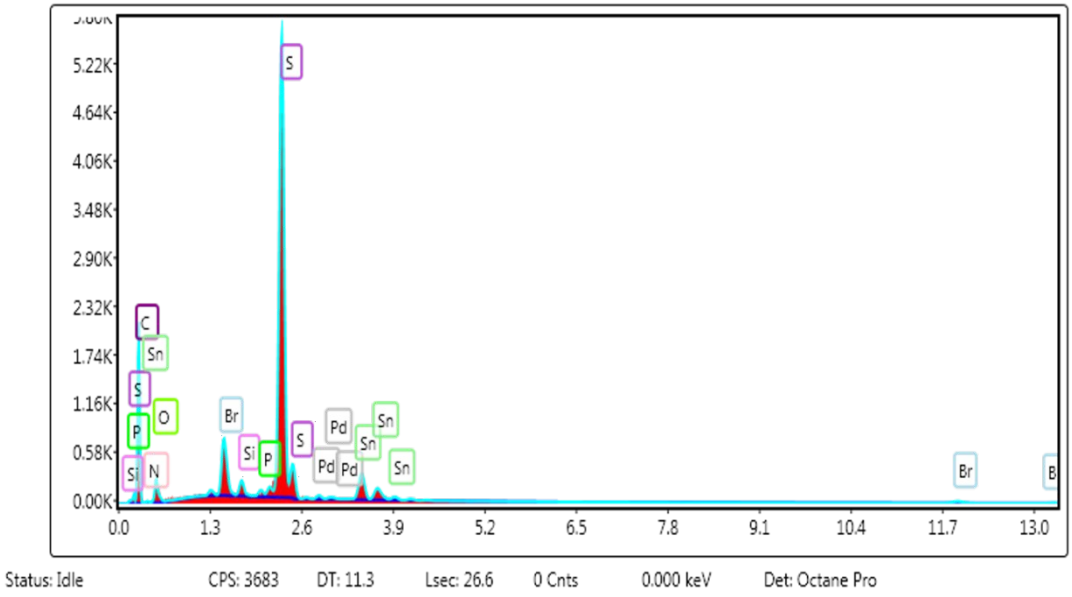


***Figure S14.*** EDX spectra of **SP-BTT.**

***Table S4.*** Elemental composition (in weight %) of obtained materials detected by EDX.

| **Sample** | **Composition** | **C (%)** | **H (%)** | **N (%)** | **S (%)** | **C:N** | **C:S** | **Cl (%)** | **Br (%)** | **Pd (%)** | **Br (%)** |
|---|---|---|---|---|---|---|---|---|---|---|---|
| **SNP-BDT1** | **Theoretical** | 59.98 | 1.68 | 11.66 | 26.68 | 5.1 | 2.2 | 0.85 | n.a. | 0.89 | 1.49 |
| | **Found** | 60.96 | n.a. | 15.05 | 15.77 | 4.1 | 3.9 | | | | |
| **SNP-BDT2** | **Theoretical** | 73.44 | 3.08 | 7.14 | 16.34 | 10.3 | 4.5 | 0.3 | 0.94 | 0.64 | 1.70 |
| | **Found** | 68.99 | n.a. | 10.23 | 12.59 | 6.7 | 5.5 | | | | |
| **SP-BTT** | **Theoretical** | 59.23 | 1.24 | n.a. | 39.53 | n.a. | 1.5 | n.a. | 3.62 | 0.54 | 5.27 |
| | **Found** | 60.74 | n.a. | 0.02 | 23.72 | n.a. | 2.6 | | | | |

**X-ray photoelectron spectroscopy (XPS).**

***Table S5.*** Elemental distribution and peak positions measured by XPS for **SNP-BDT1**.

| Name | Peak BE | FWHM eV | Area (P) CPS.eV | Atomic% | Q |
|---|---|---|---|---|---|
| **Si2p** | 104.65 | 3.79 | 40808.94 | 2.1 | 1 |
| **P2p** | 139.28 | 3.06 | 5121.06 | 0.18 | 1 |
| **S2p** | 164.59 | 2.92 | 401616.07 | 10.23 | 1 |
| **Cl2p** | 199.7 | 3.23 | 8850.33 | 0.16 | 1 |
| **C1s** | 285.41 | 2.89 | 1397336.88 | 72.09 | 1 |
| **Pd3d** | 337.74 | 3.01 | 34396.94 | 0.09 | 1 |
| **N1s** | 399.34 | 2.79 | 253441.79 | 8.42 | 1 |
| **Sn3d** | 487.59 | 2.87 | 161993.59 | 0.26 | 1 |
| **O1s** | 533.55 | 3.81 | 302954.26 | 6.47 | 1 |

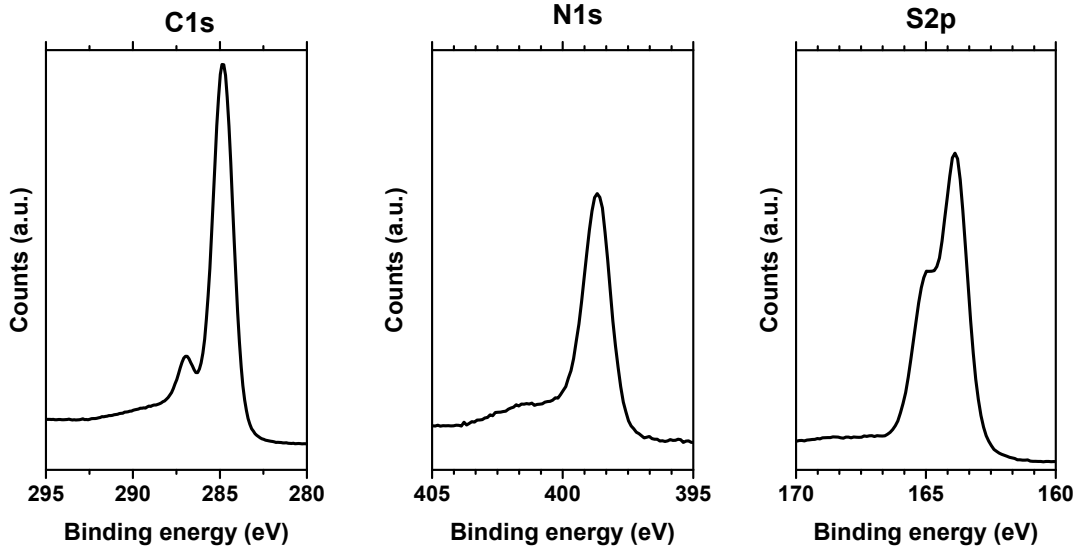


***Figure S15.*** XPS C1s, N1s and S2p signals in **SNP-BDT1** network**.**

***Table S6.*** Elemental distribution and peak positions measured by XPS for **SNP-BDT2**.

| Name | Peak BE | FWHM eV | Area (P) CPS.eV | Atomic% | Q |
|---|---|---|---|---|---|
| **Br3d** | 70.68 | 3.51 | 16843.96 | 0.25 | 1 |
| **Si2p** | 104.52 | 3.62 | 60689.57 | 2.76 | 1 |
| **S2p** | 164.57 | 2.83 | 259694.31 | 5.85 | 1 |
| **C1s** | 285.34 | 2.69 | 1680479.87 | 76.61 | 1 |
| **Pd3d** | 337.62 | 1.72 | 6139.45 | 0.01 | 1 |
| **N1s** | 399.25 | 1.66 | 182631.16 | 5.36 | 1 |
| **Sn3d** | 487.53 | 3.17 | 278032.66 | 0.39 | 1 |
| **O1s** | 533.47 | 3.6 | 464557.16 | 8.77 | 1 |

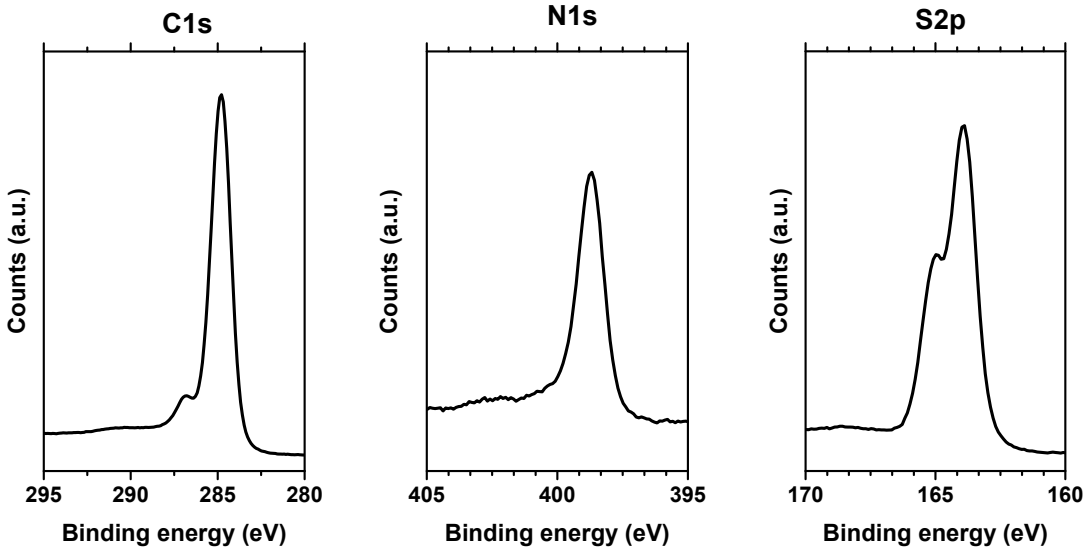


***Figure S16.*** XPS C1s, N1s and S2p signals in **SNP-BDT2** network**.**

***Table S7.*** Elemental distribution and peak positions measured by **XPS for SP-BTT**.

| Name | Peak BE | FWHM eV | Area (P) CPS.eV | Atomic% | Q |
|---|---|---|---|---|---|
| **Br3d** | 70.77 | 3.68 | 42101.33 | 0.87 | 1 |
| **Si2p** | 104.43 | 3.3 | 42101.33 | 3.1 | 1 |
| **S2p** | 164.55 | 2.89 | 42101.33 | 16 | 1 |
| **Cl2s** | 269.92 | 4.31 | 42101.33 | 0.9 | 1 |
| **C1s** | 285.2 | 1.3 | 42101.33 | 66.83 | 1 |
| **Pd3d** | 337.55 | 2.62 | 42101.33 | 0.04 | 1 |
| **N1s** | 401.6 | 3.28 | 42101.33 | 0.93 | 1 |
| **Sn3d** | 487.49 | 2.8 | 42101.33 | 0.6 | 1 |
| **O1s** | 533.37 | 3.6 | 42101.33 | 10.73 | 1 |

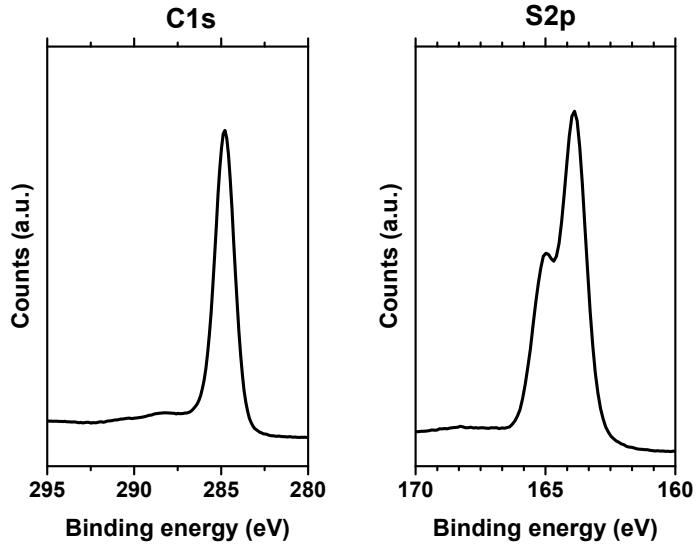


***Figure S17.*** XPS C1s and S2p signals in **SP-BTT** network**.**

**Solid-state UV-Vis study and optical bandgap calculations.**

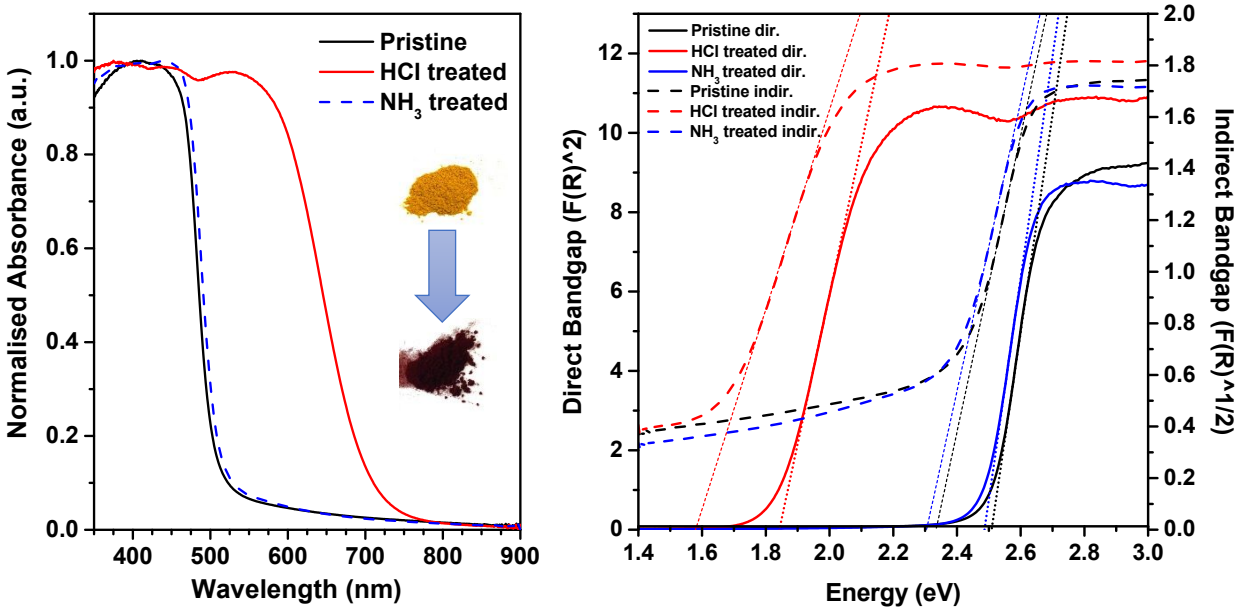


***Figure S18.*** Solid-state UV-Vis spectra (left), in the inset – photographs of polymers before (up) and after (down) HCl treatment, and Tauc plots for in-/direct optical bandgap estimation using Kubelka-Munk theory (right) of **SNP-NDT2.**

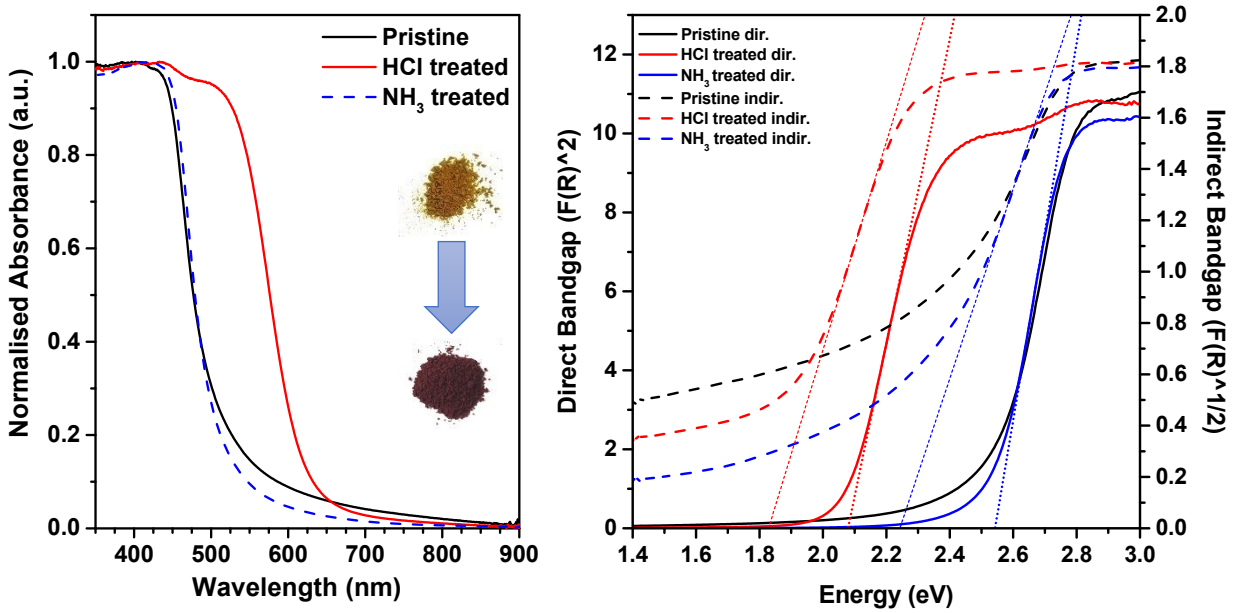


***Figure S19.*** Solid-state UV-Vis spectra (left), in the inset – photographs of polymers before (up) and after (down) HCl treatment, and Tauc plots for in-/direct optical bandgap estimation using Kubelka-Munk theory (right) of **SNP-BTT1.**

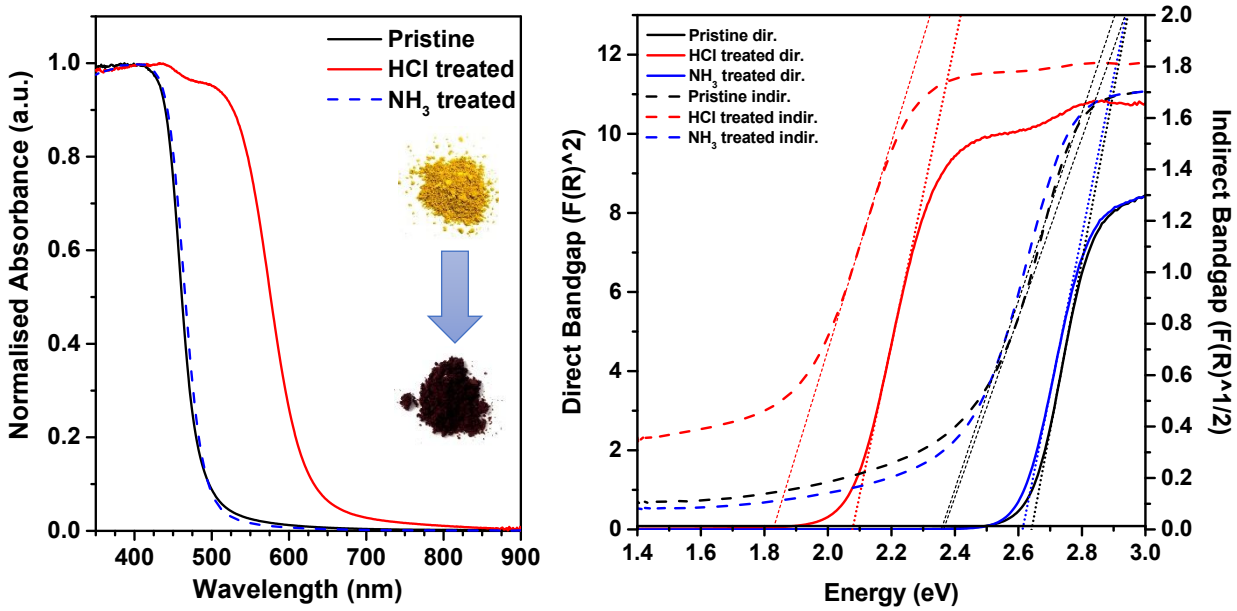


***Figure S20.*** Solid-state UV-Vis spectra (left), in the inset – photographs of polymers before (up) and after (down) HCl treatment, and Tauc plots for in-/direct optical bandgap estimation using Kubelka-Munk theory (right) of **SNP-BTT2**.

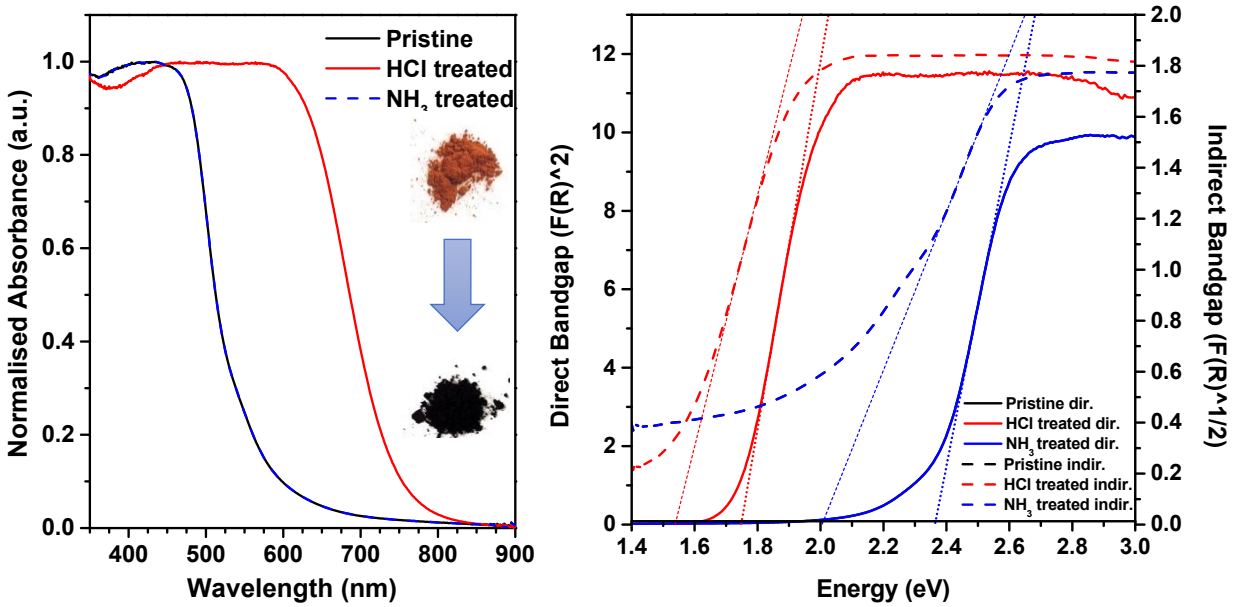


***Figure S21.*** Solid-state UV-Vis spectra (left), in the inset – photographs of polymers before (up) and after (down) HCl treatment, and Tauc plots for in-/direct optical bandgap estimation using Kubelka-Munk theory (right) of **SNP-BDT1.**

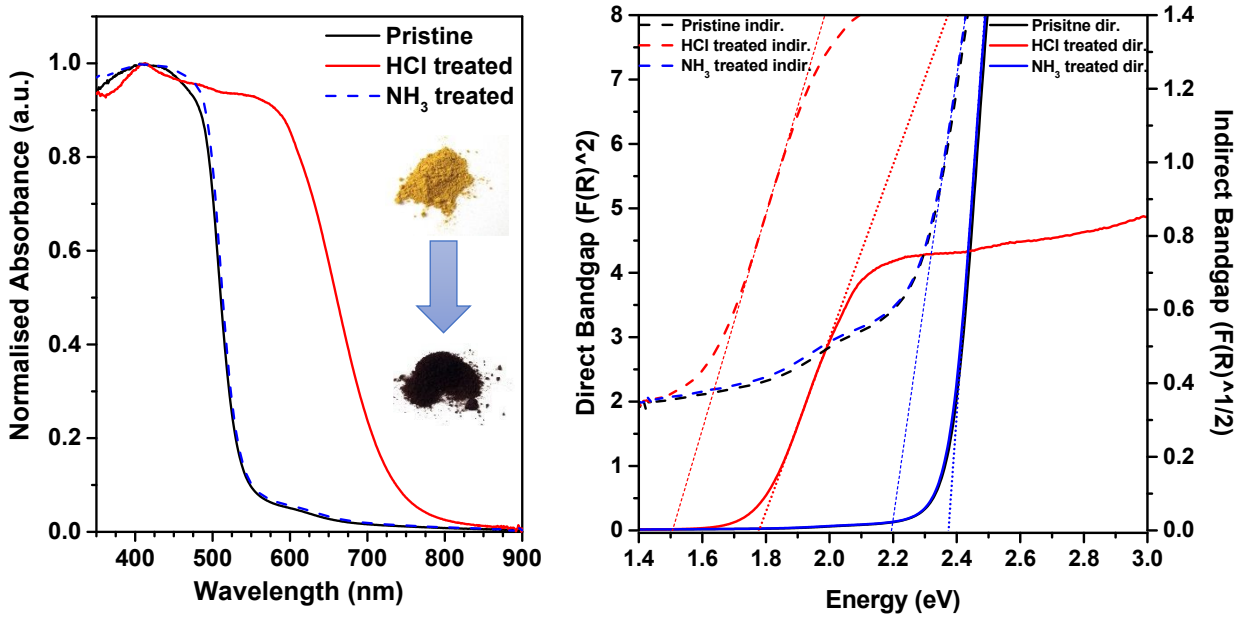


***Figure S22.*** Solid-state UV-Vis spectra (left), in the inset – photographs of polymers before (up) and after (down) HCl treatment, and Tauc plots for in-/direct optical bandgap estimation using Kubelka-Munk theory (right) of **SNP-BDT2.**

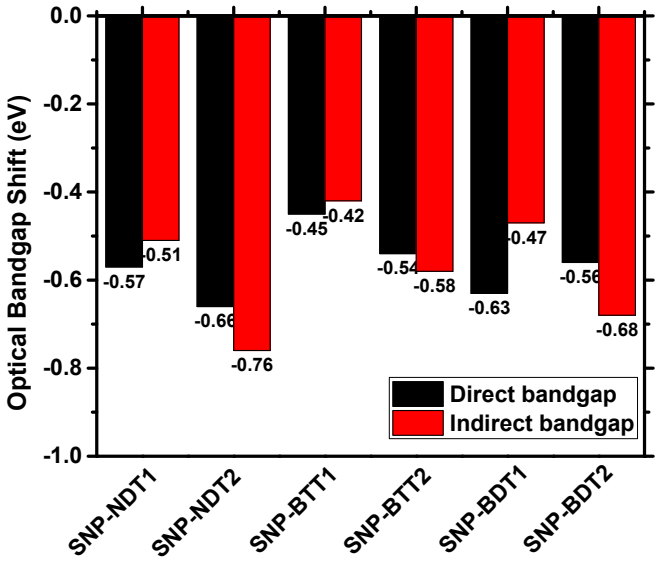


***Figure S23.*** Change in the in-/direct optical bandgap after exposure of prepared SNPs to HCl vapour.

**HCl vapour concentration study and polymer stability test.**

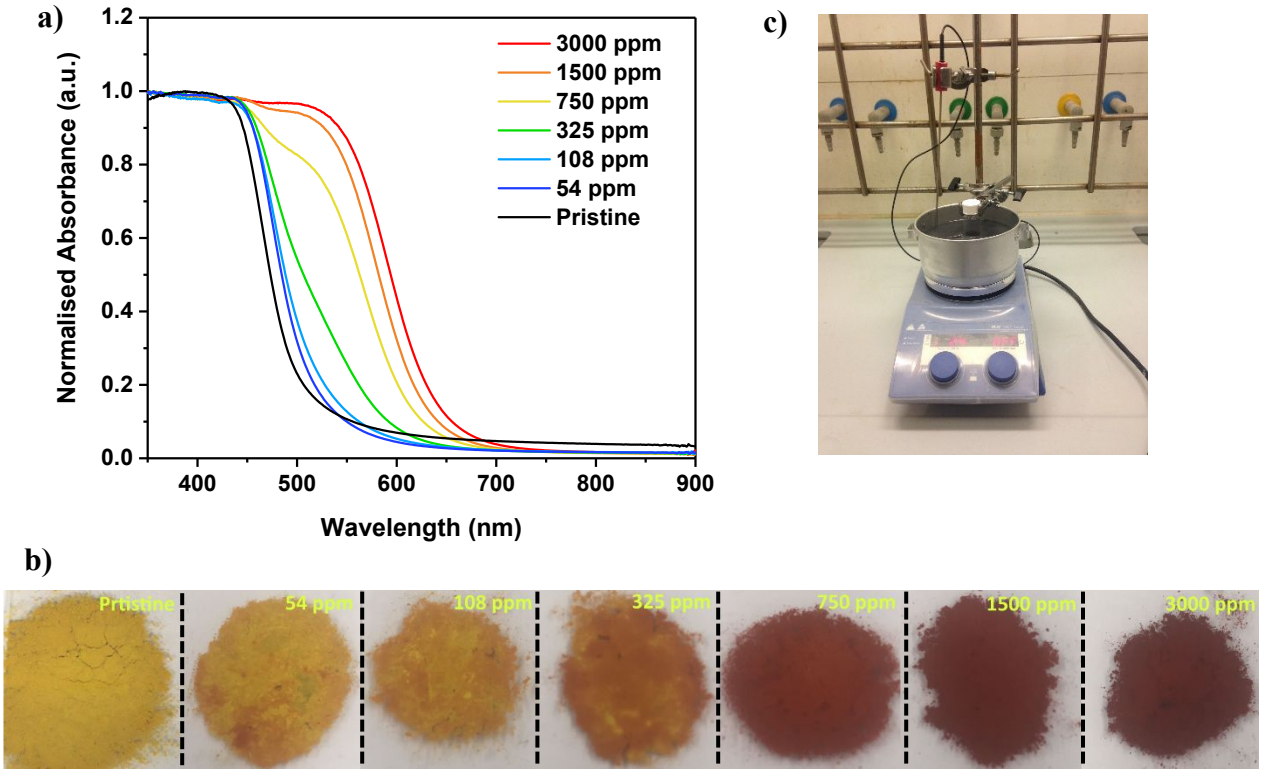


***Figure S24.*** HCl vapour concentration study, performed at 25 °C, of **SNP-NDT1** showing solid-state UV-Vis spectra (a) and photographs (b) of samples exposed to following HCl vapour concentrations: 3000 ppm, 1500 ppm, 750 ppm, 325 ppm, 108 ppm, 54 ppm and 0 ppm (pristine sample); c) experimental setup.

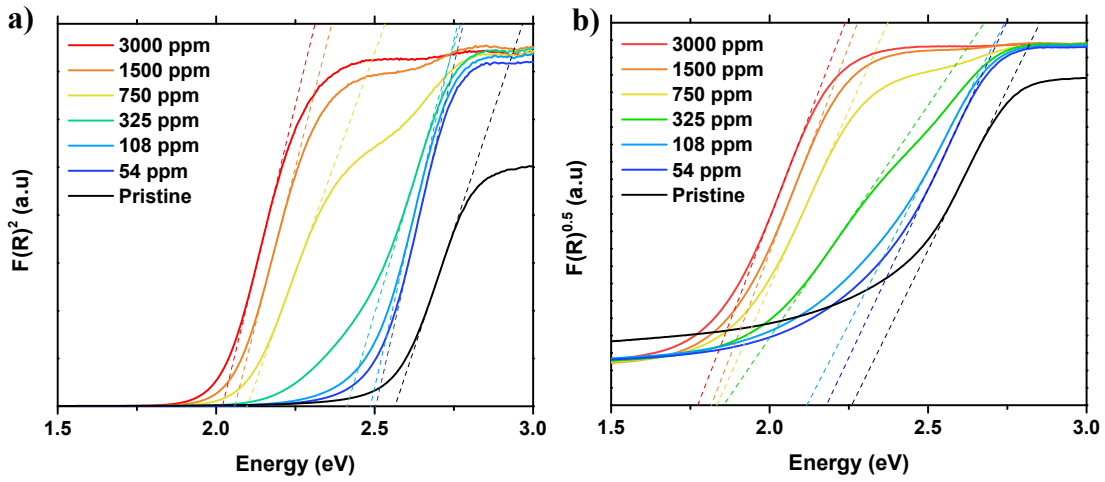


***Figure S25.*** Tauc plots for direct (a) and indirect (b) optical bandgaps of **SNP-NDT1** exposed to different HCl vapour concentrations.

***Table S8.*** Direct and indirect optical bandgaps of **SNP-NDT1** exposed to different HCl vapour concentrations.

| HCl vapour concentration | Direct bandgap (eV) | Indirect bandgap (eV) |
|---|---|---|
| 3000 | 2.02 | 1.77 |
| 1500 | 2.06 | 1.81 |
| 750 | 2.1 | 1.83 |
| 325 | 2.41 | 1.85 |
| 108 | 2.48 | 2.12 |
| 54 | 2.5 | 2.18 |
| Pristine | 2.56 | 2.27 |

**Experimental details.**

For HCl detection limit samples of **SNP-NDT1** polymer were exposed to vapours of hydrochloric acid in temperature-controlled environment by keeping the reaction vial in the oil bath (25 $^{o}$C monitored with a thermometer). Smaller vial with sample was introduced inside the reaction vial containing necessary amount of HCl. Samples were exposed for 30 s and further subjected to solid-state UV-Vis measurements without any delays.

HCl vapour concentration in ppm was calculated by following equation:

$$ppm\ (HCl)\ = \frac{\mu g\ (HCl\ vapor)}{g\ (air)}$$

Molar mass of the air inside the reaction vial was determined using ideal gas law:

$$\boldsymbol{n}\ (air) = \frac{\boldsymbol{P}\ (atm) * \boldsymbol{Vvial}(L)}{\boldsymbol{R}(L * atm/l * mol) * \boldsymbol{T}(K)} = \frac{1 * 0.03}{0.082 * 298} = \mathbf{1.23}\ mmol$$

were $\boldsymbol{Vvial}$ – is the volume the reaction vial and equals to 30 mL or 0.03 L.

Mass of the air inside the reaction vial was determined as follows:

$$\boldsymbol{m}(air) = \boldsymbol{n}(air) * \boldsymbol{M}(air) = 1.23\ mmol\ * 28.97 g\ mol - 1 = \mathbf{0.036}\ g$$

***Table S9.*** Correlation between volume of 35% solution and concentration of HCl.

| µL 35% HCl | ppm |
|---|---|
| 259.2 | 3000 |
| 129.6 | 1500 |
| 64.8 | 750 |
| 32.4 | 325 |
| 10.8 | 108.3 |

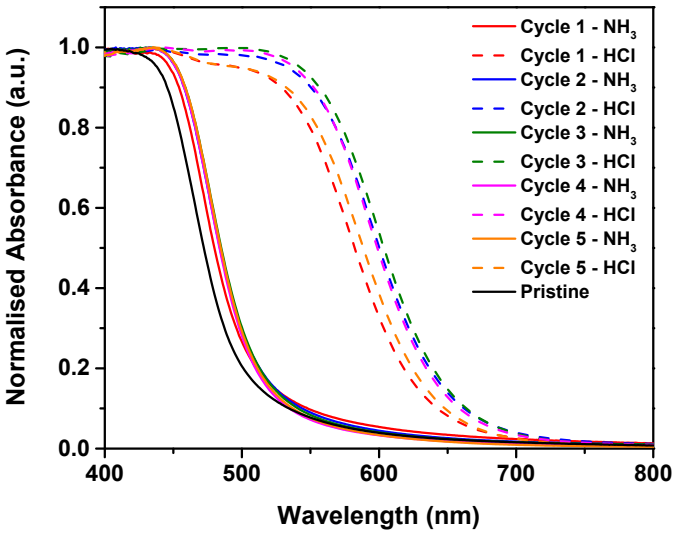


***Figure S26.*** Stability test of SNP-NDT1 showing solid-state UV-Vis spectra for five consecutive HCl/$NH_3$ treatment cycles.

**Screening of different acids.**

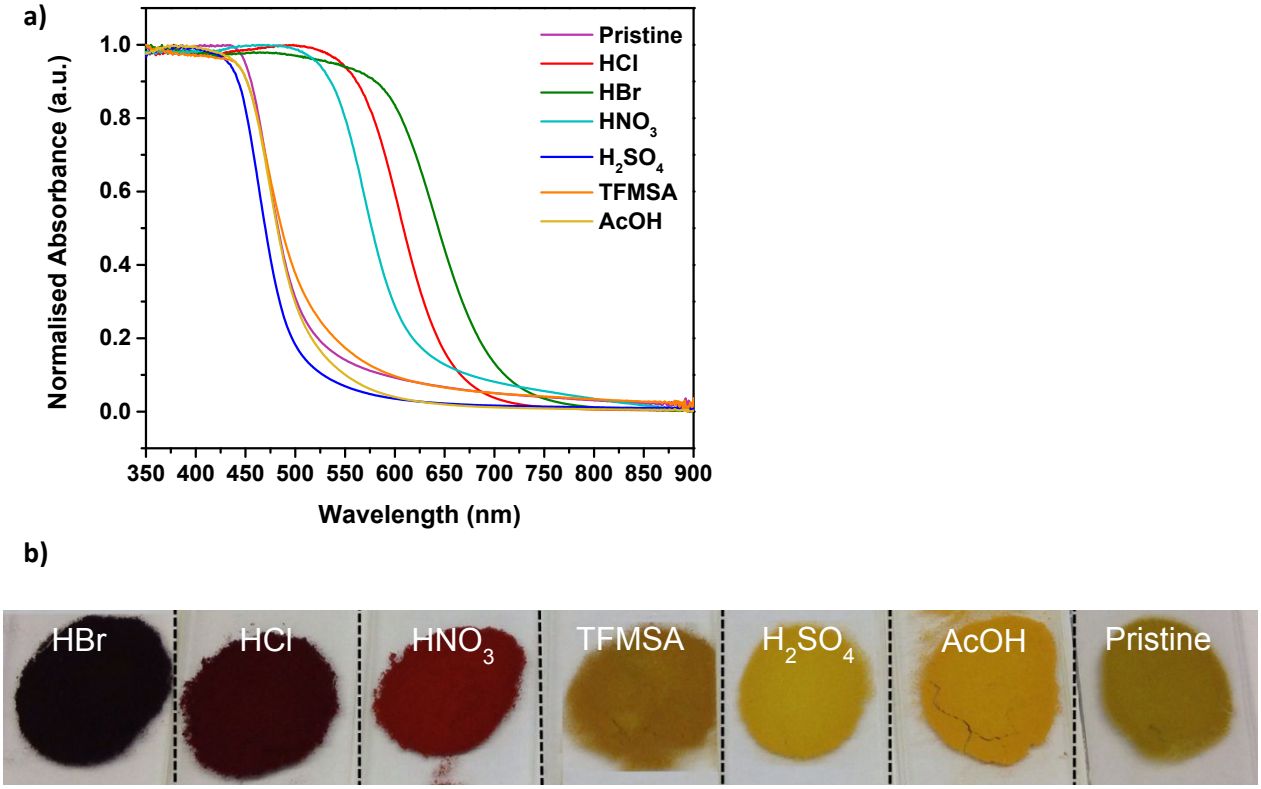


***Figure S27.*** Exposure **of SNP-NDT1** polymer to vapours of different acids: a) solid-state UV-Vis spectra; b) photographs of the material after 3 days exposure experiment.

**Fourier-transform infrared spectroscopy (FTIR) study.**

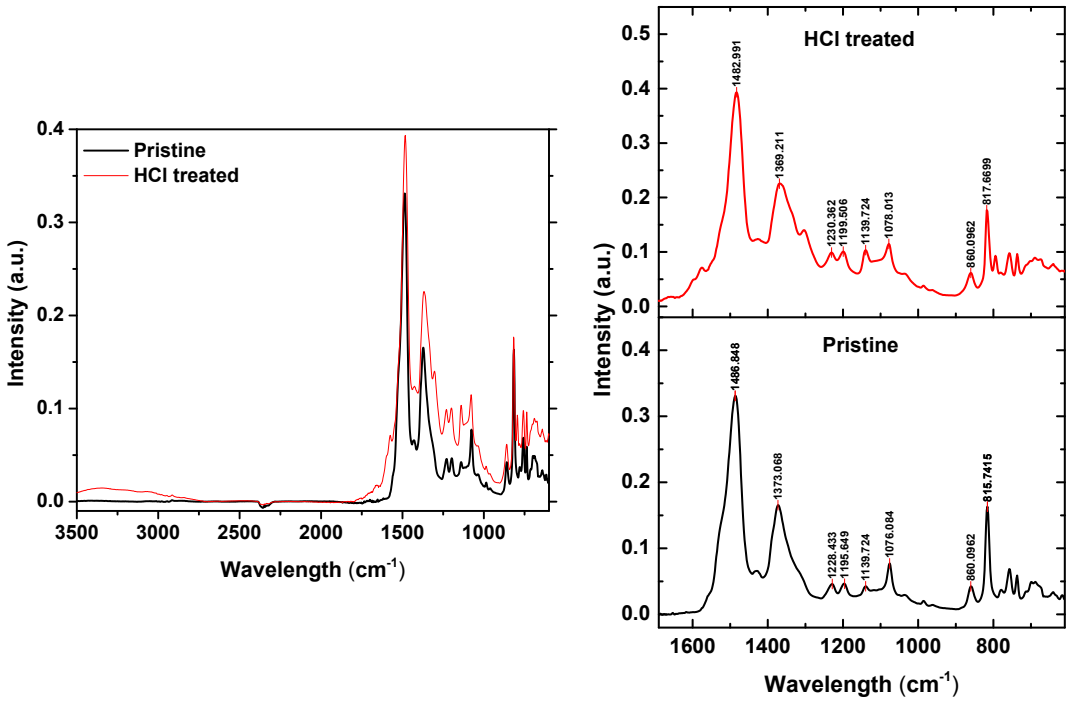


***Figure S28.*** FTIR spectra – whole range (left) and 600-1700 $cm^{-1}$ region (right) – of **SNP-NDT1** in pristine state (black) and after treatment with HCl vapour (red).

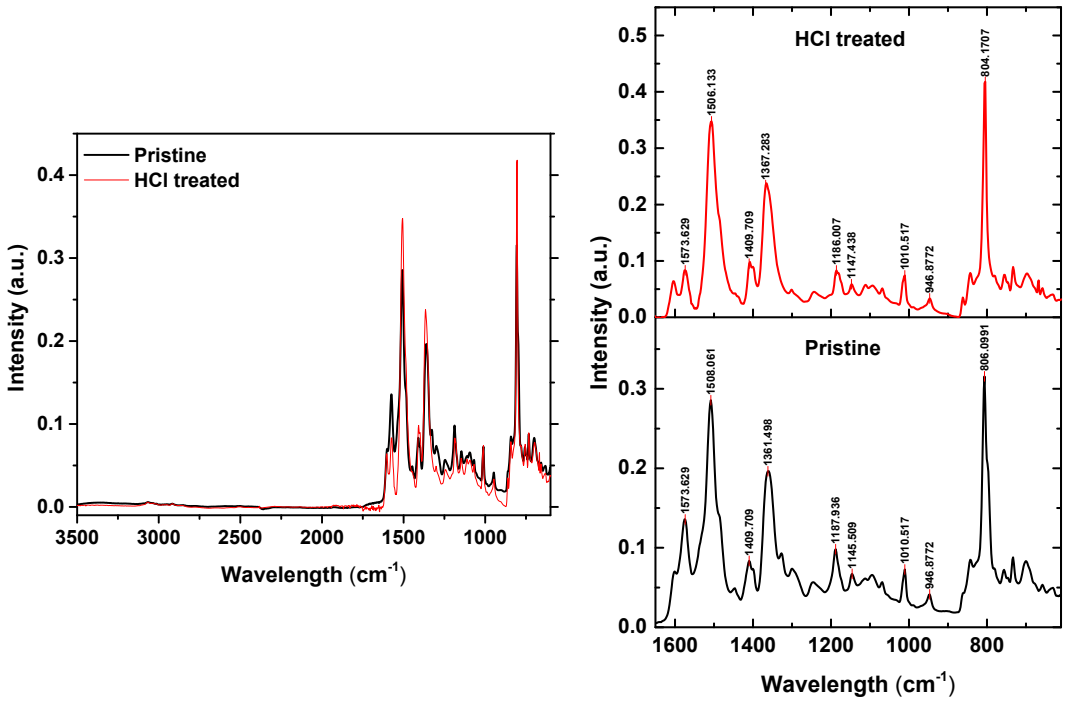


***Figure S29.*** FTIR spectra – whole range (left) and 600-1700 $cm^{-1}$ region (right) – of **SNP-NDT2** in pristine state (black) and after treatment with HCl vapour (red).

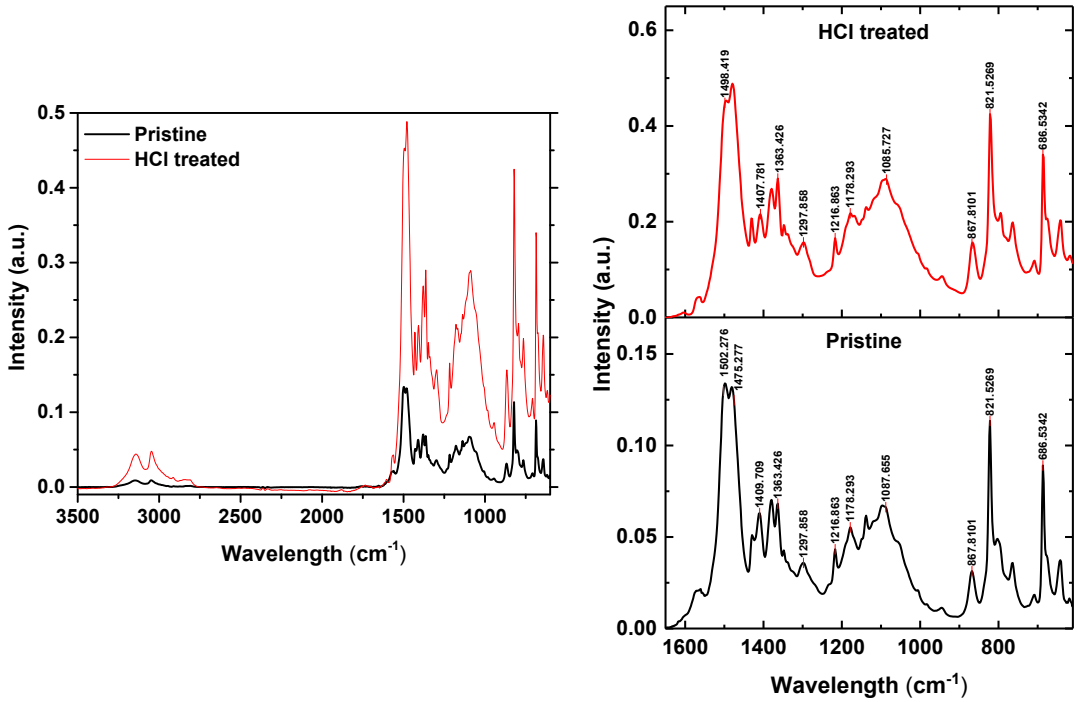


***Figure S30.*** FTIR spectra – whole range (left) and 600-1700 $cm^{-1}$ region (right) – of **SNP-BTT1** in pristine state (black) and after treatment with HCl vapour (red).

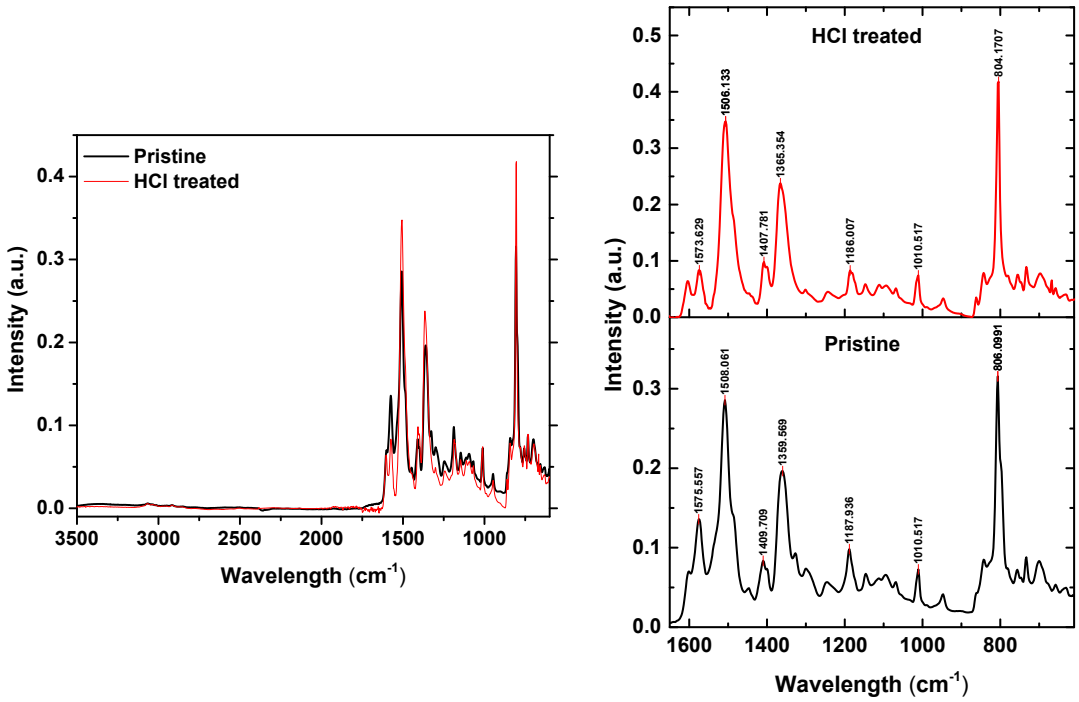


***Figure S31***. FTIR spectra – whole range (left) and 600-1700 $cm^{-1}$ region (right) – of **SNP-BTT2** in pristine state (black) and after treatment with HCl vapour (red).

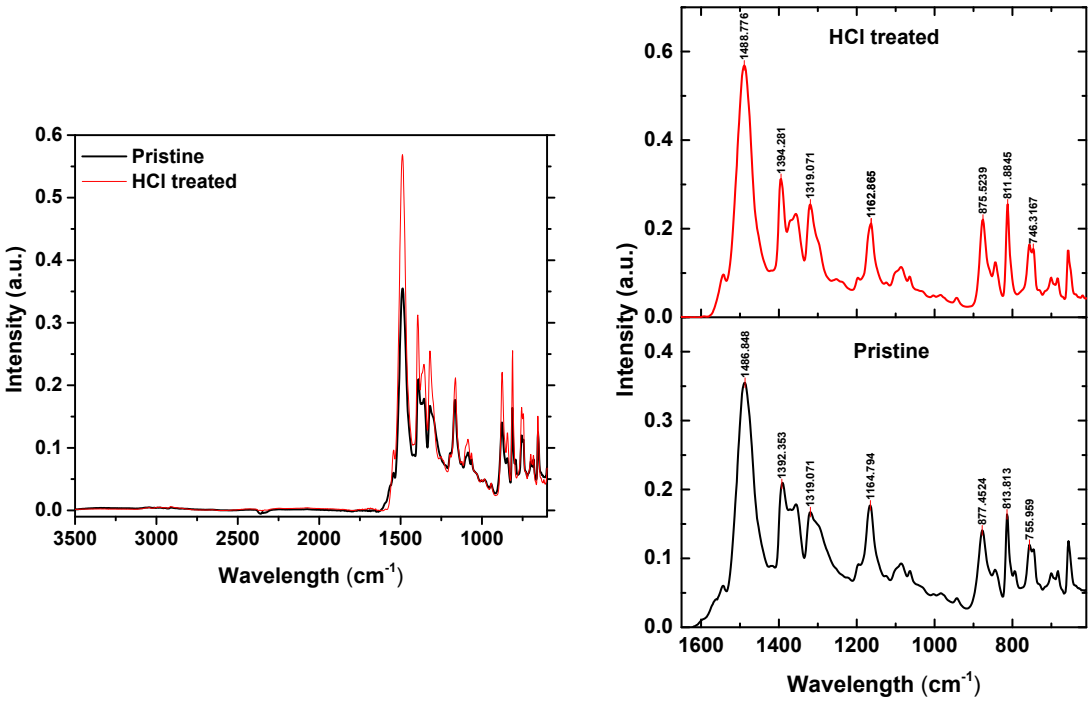


***Figure S32.*** FTIR spectra – whole range (left) and 600-1700 $cm^{-1}$ region (right) – of **SNP-BDT1** in pristine state (black) and after treatment with HCl vapour (red).

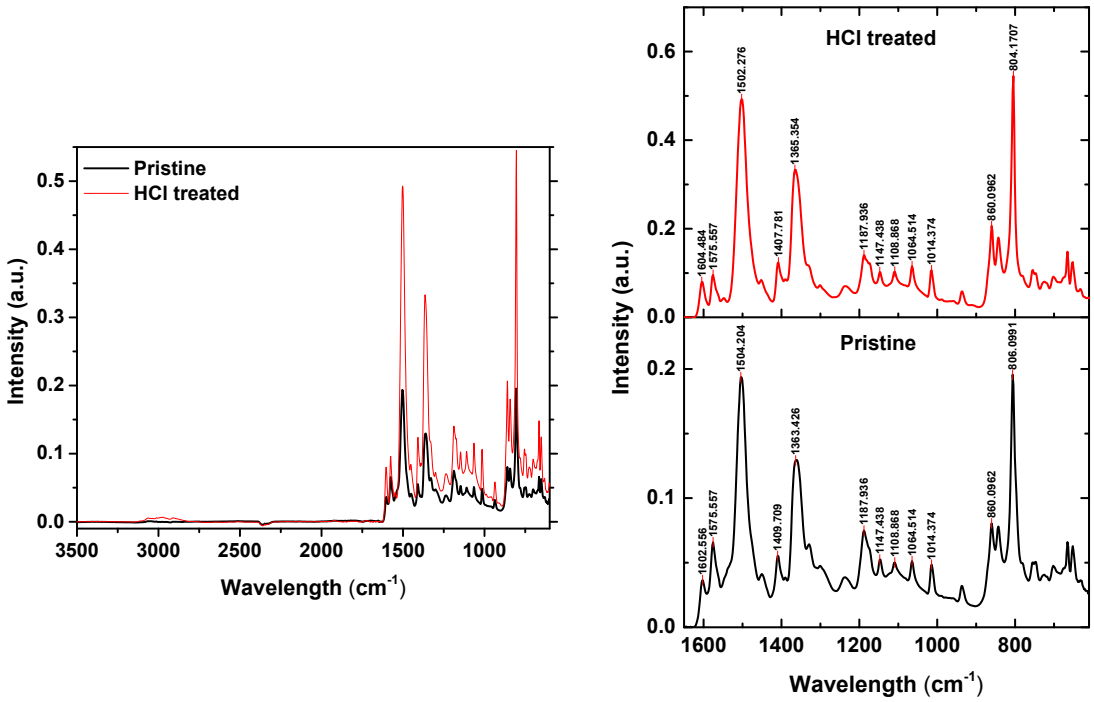


***Figure S33.*** FTIR spectra – whole range (left) and 600-1700 $cm^{-1}$ region (right) – of **SNP-BDT2** in pristine state (black) and after treatment with HCl vapour (red).

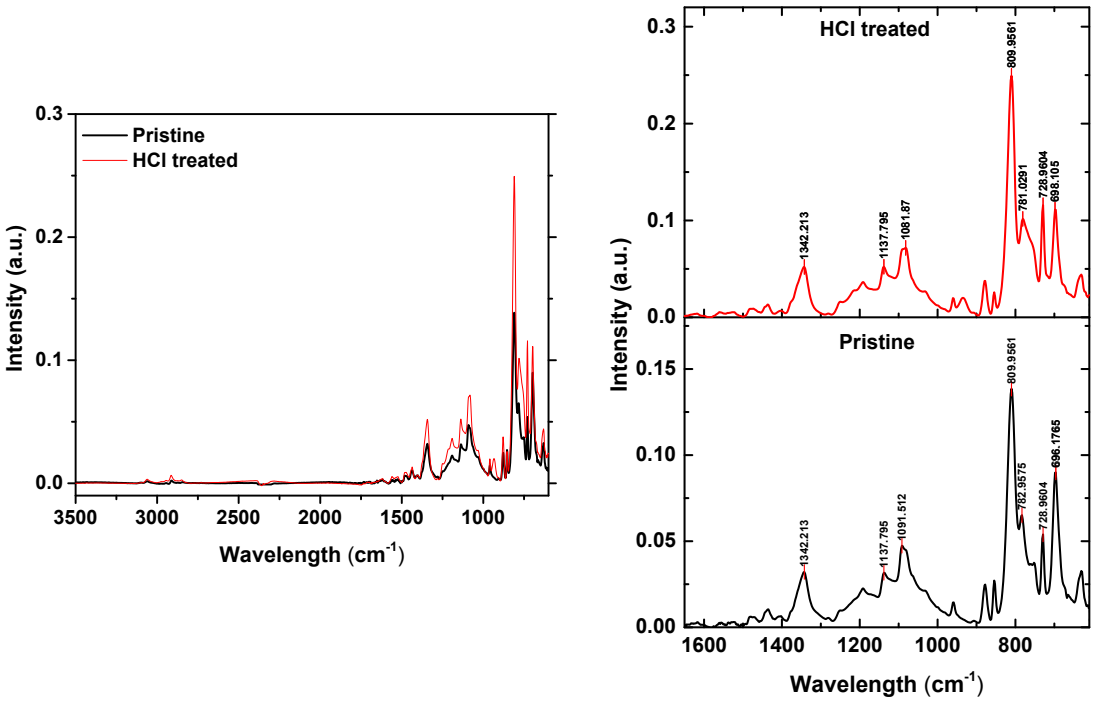


***Figure S34.*** FTIR spectra– whole range (left) and 600-1700 $cm^{-1}$ region (right) – of **SP-BTT** in pristine state (black) and after treatment with HCl vapour (red).

**Complimentary stability study for SNPs (in addition to SNP-NDT1 cycling tests)**

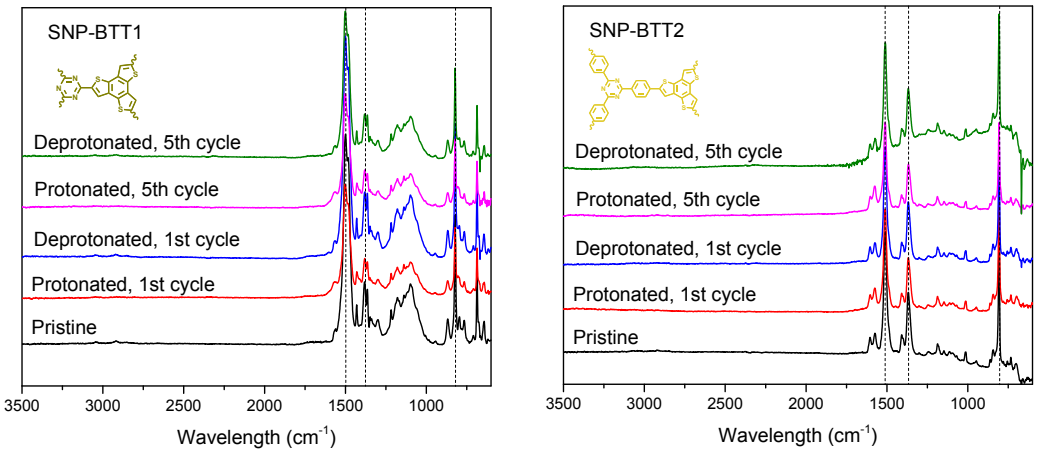

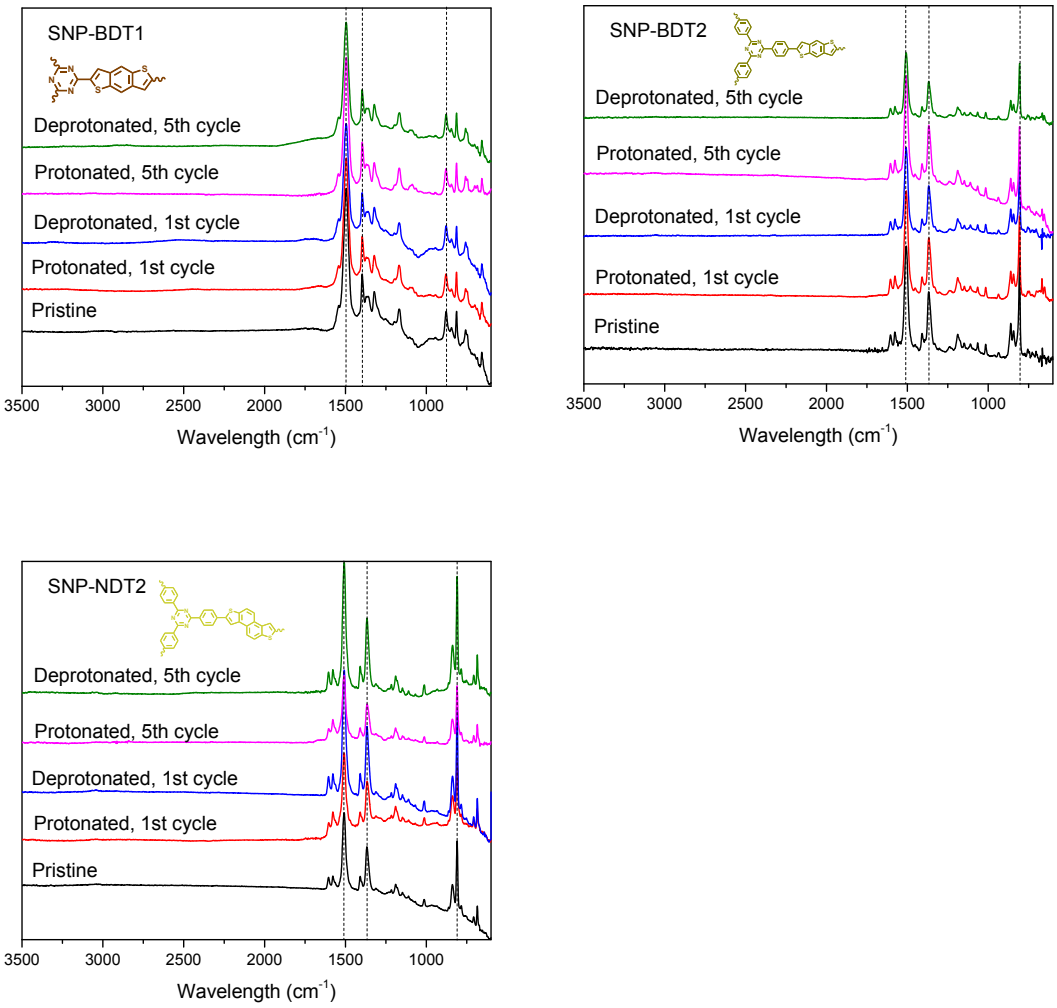


***Figure S35.*** FTIR spectra of **SNP-BTT1, SNP-BTT2, SNP-BDT1, SNP-BDT2** and **SNP-NDT2** recorded at pristine state and after 1st and 5th $HCl/NH_3$ cycle.

**Solid state photoluminescence (PL) measurements.**

***Table S10.*** Absolute quantum yield (AQY) measurements data for prepared materials.

| Polymer | AQY (%) at 365 nm | Absorbance (%) | λexc (nm) | λexc (counts) | λem (nm) | λem (counts) |
|---|---|---|---|---|---|---|
| **SNP-NDT1** | 0.5 | 62.6 | 364.67 | 23418.32 | 402.49 | 23.06 |
| **SNP-NDT2** | 1.0 | 78.0 | 364.67 | 13777.95 | 541.59 | 16.14 |
| **SNP-BTT1** | 0.5 | 80.4 | 364.67 | 12332.56 | 408.54 | 31.13 |
| **SNP-BTT2** | 0.6 | 77.7 | 364.67 | 13901.78 | 404.76 | 13.52 |
| **SNP-BDT1** | 0.3 | 79.5 | 364.67 | 12854.86 | 403.25 | 13.82 |
| **SNP-BDT1** | 0.1 | 81.4 | 364.67 | 11751.17 | 560.28 | 16.7 |
| **SP-BTT** | 0.5 | 56.1 | 363.91 | 28154.38 | 403.25 | 26.9 |


***Figure S36.*** Photograph of obtained SNPs and **SP-BTT** under UV light irradiation ($\lambda_{exc}$ = 365 nm).

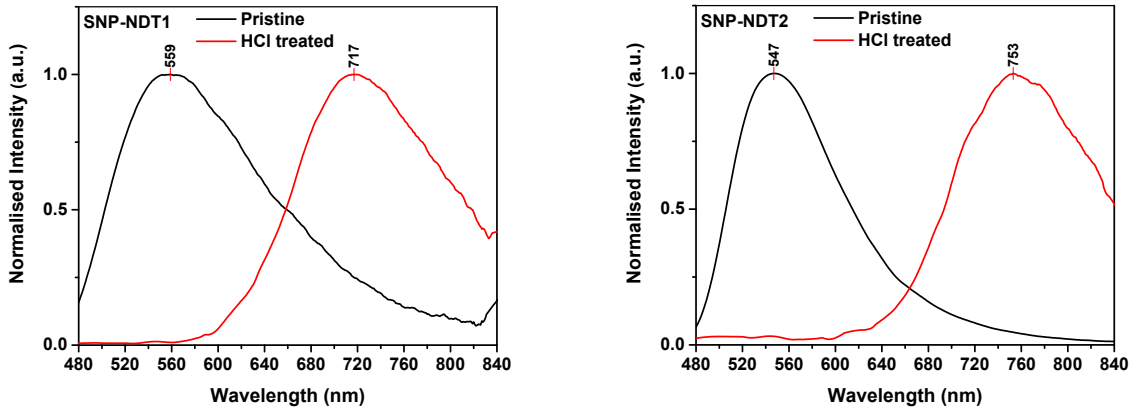

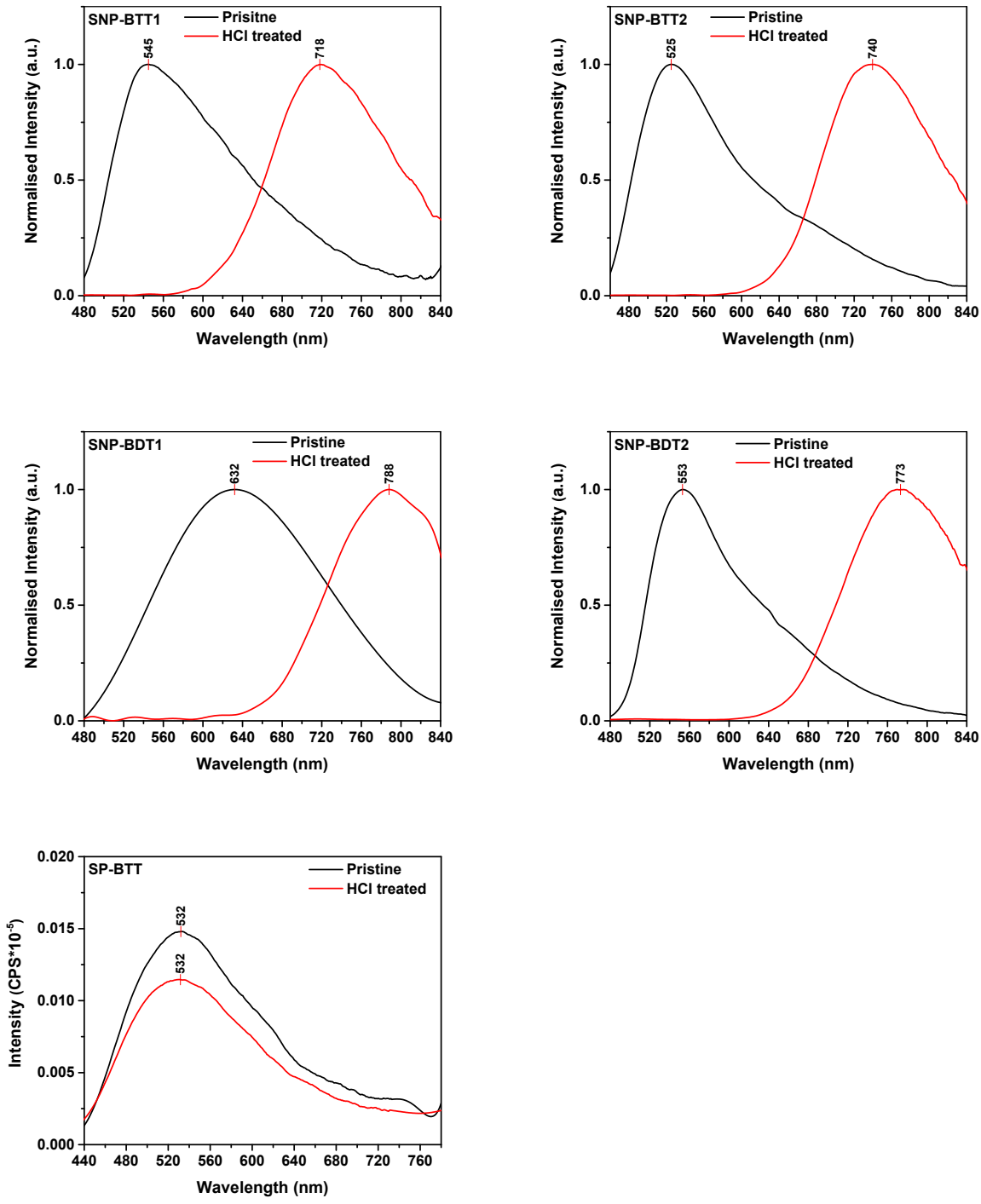


***Figure S37.*** PL spectra of pristine (black) and HCl treated (red) materials ($\lambda_{exc}$ = 420 nm).

**Time-correlated single-photon counting (TCSPC) measurement**

***Table S11.*** TCSPC data for obtained materials.

| Polymer | $\lambda_{em}$ (nm) | $\tau_1$ (ns) | $B_1$ | $\tau_2$ (ns) | $B_2$ | $\tau_3$ (ns) | $B_3$ | $\tau_{avg}$ (ns) |
|---|---|---|---|---|---|---|---|---|
| **SNP-NDT1** | 559 | 0.18 | 46.09 | 0.61 | 42.85 | 2.16 | 11.06 | 0.58 |
| **SNP-NDT1-HCl** | 717 | 1.09 | 46.98 | 0.28 | 41.53 | 4.21 | 11.50 | 1.11 |
| **SNP-NDT2** | 547 | 0.92 | 42.04 | 3.84 | 16.46 | 1.93 | 41.50 | 1.06 |
| **SNP-NDT2-HCl** | 753 | 2.25 | 30.66 | 9.68 | 9.90 | 0.33 | 59.44 | 1.85 |
| **SNP-BTT1** | 545 | 0.60 | 33.54 | 2.82 | 9.83 | 0.11 | 56.62 | 0.54 |
| **SNP-BTT1-HCl** | 718 | 1.38 | 45.19 | 7.02 | 16.32 | 0.31 | 38.50 | 1.89 |
| **SNP-BTT2** | 525 | 0.47 | 31.61 | 2.22 | 7.54 | 0.09 | 60.85 | 0.37 |
| **SNP-BTT2-HCl** | 740 | 1.29 | 49.45 | 0.32 | 39.41 | 5.07 | 11.14 | 1.33 |
| **SNP-BDT1** | 632 | 0.53 | 29.66 | 1.98 | 7.02 | 0.12 | 63.32 | 0.41 |
| **SNP-BDT1-HCl** | 788 | 1.06 | 28.44 | 5.72 | 9.54 | 0.29 | 62.02 | 1.03 |
| **SNP-BDT2** | 553 | 0.58 | 39.33 | 2.25 | 12.74 | 0.12 | 47.94 | 0.57 |
| **SNP-BDT2-HCl** | 773 | 0.79 | 41.03 | 3.76 | 17.22 | 0.13 | 41.75 | 1.03 |
| **SP-BTT** | 532 | 0.57 | 29.66 | 1.98 | 7.02 | 0.12 | 63.32 | 0.37 |
| **SP-BTT-HCl** | 532 | 0.14 | 41.39 | 0.56 | 50.37 | 1.89 | 8.24 | 0.49 |

Fluorescence life-times for pristine and HCl-treated polymers in in solid state were obtained from TCSPC decays by triple exponential, which yield $\tau_1$, $\tau_2$, and $\tau_3$ according to $\sum_{i=1}^{n}\left(A + B_i * \left(-t/\tau_i\right)\right)$. $\tau_{AVG}$ is the weighted average lifetime calculated as $\sum_{i=1}^{n} B_i * \tau_i$, where $B_i$ is the relative amplitude.

**Electronic conductivity measurements.**

The current-voltage characteristics of SNPs and **SP-BTT** were studied by a two-probe method. Powder samples were loaded in a plastic cylinder (diameter: 8 mm) and compressed into a pellet between two stainless rods with pressure of ~50 bar (Figure S45). In a typical experiment, a bias sweep of -10 to 10 V was applied using a Keithley 2612 A source meter, and the current through the rods and the sample was recorded. Minimum triplicates for each sample were conducted, and the average was taken for estimation of the conductivity. The conductivity ($\rho$) was calculated based on the following equation: $R = \frac{V}{I} = \rho\frac{l}{A}$ , where $l$ is the sample thickness (determined by optical microscope imaging) as the conduction path length and $A$ is the cross-sectional area of the cylinder. The freshly exposed to HCl vapours (35% aqueous solution) and $NH_3$ vapours (24% aqueous solution) samples were tested right away without any delays.

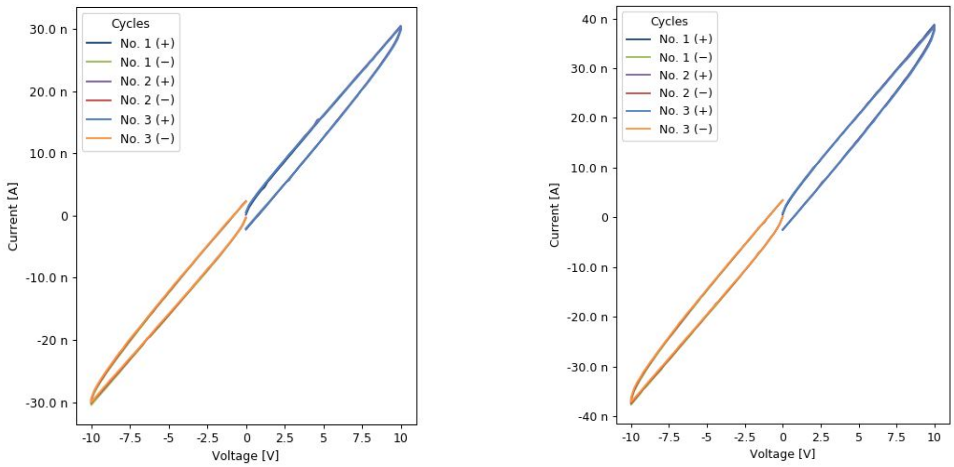


***Figure S38.*** I-V curve recorded after three current cycles for pristine (right) and protonated (left) forms of **SNP-NDT1.**

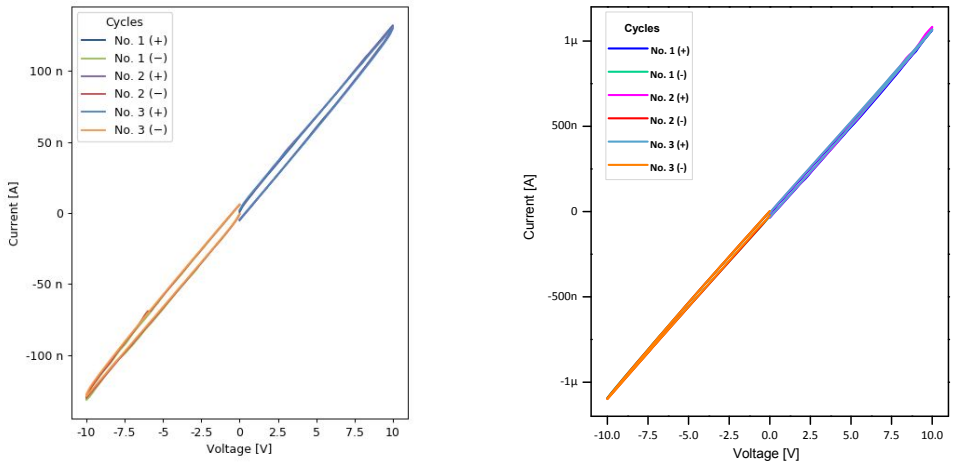


***Figure S39.*** I-V curve recorded after three current cycles for pristine (right) and protonated (left) forms of **SNP-NDT2.**

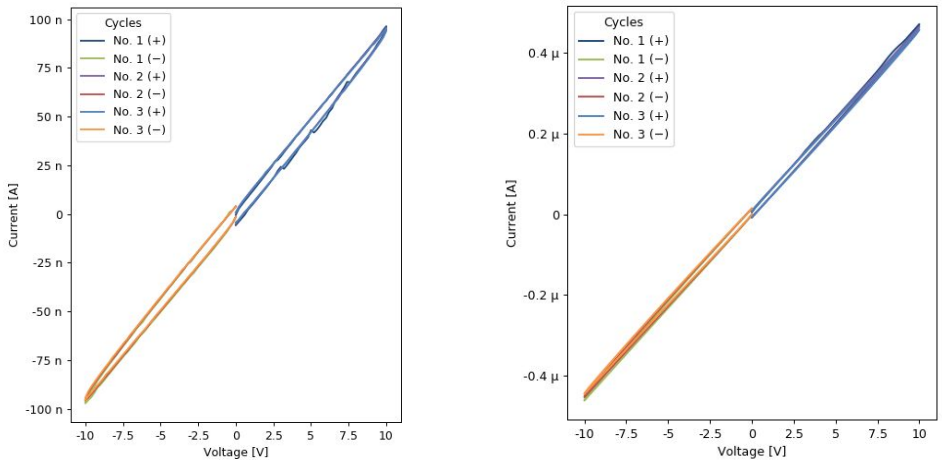


***Figure S40.*** I-V curve recorded after three current cycles for pristine (right) and protonated (left) forms of **SNP-BTT1.**

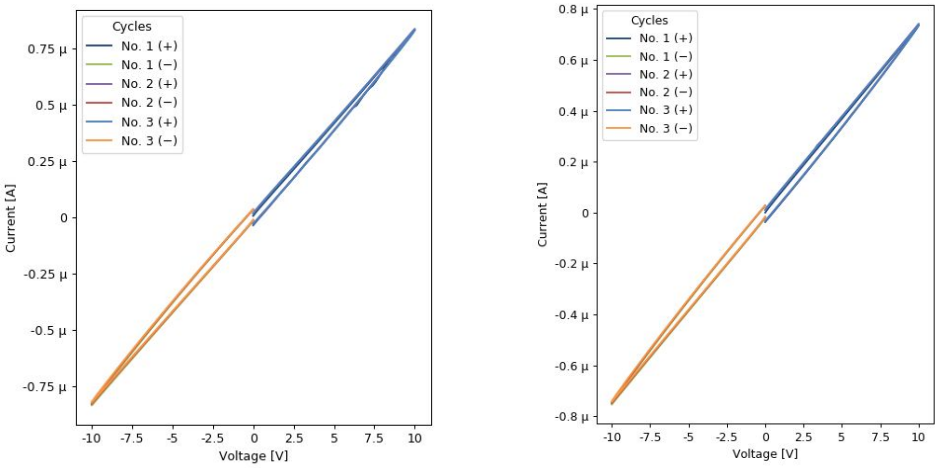


***Figure S41.*** I-V curves recorded after three current cycles for pristine (right) and protonated (left) forms of **SNP-BTT2**.

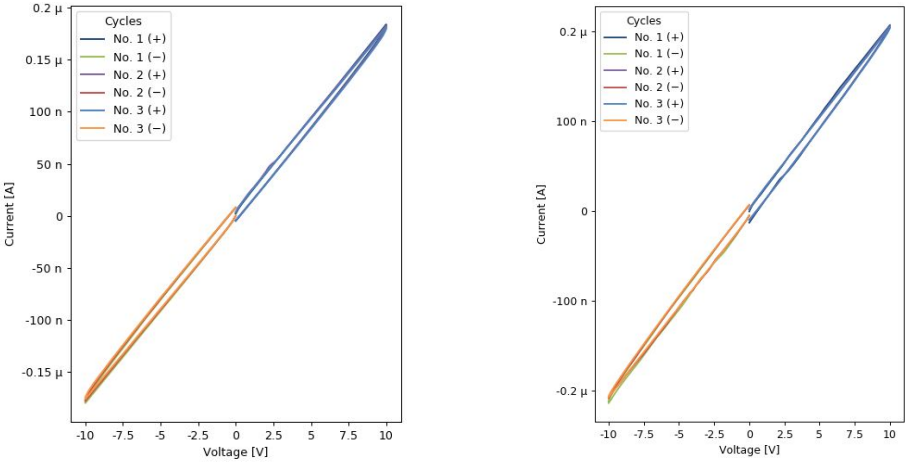


***Figure S42.*** I-V curves recorded after three current cycles for pristine (right) and protonated (left) forms of **SNP-BDT1.**

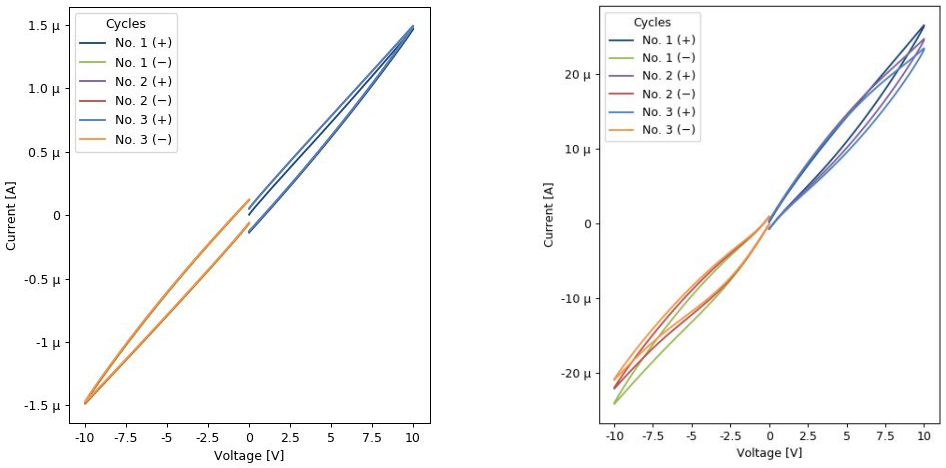


***Figure S43.*** I-V curves recorded after three current cycles for pristine (right) and protonated (left) forms of **SNP-BDT2.**

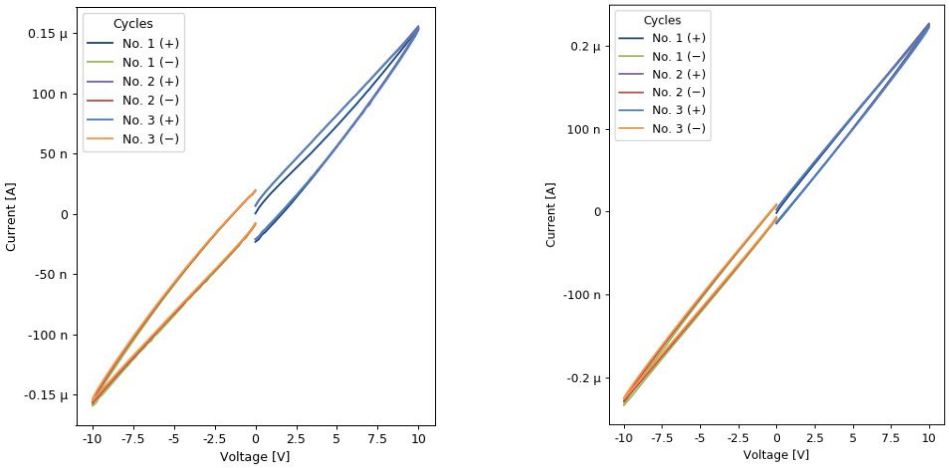


***Figure S44.*** I-V curves recorded after three current cycles for pristine (right) and protonated (left) forms of **SP-BTT.**

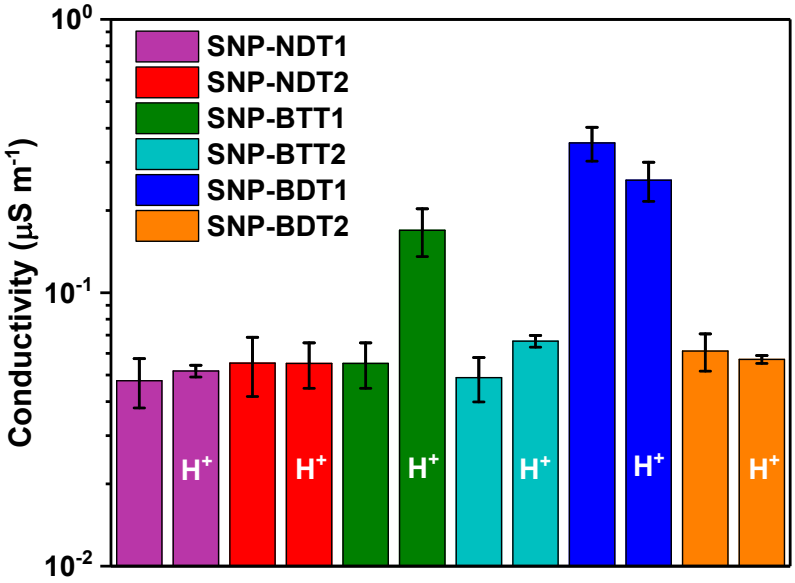


***Figure S45.*** Overview of electronic conductivity measurements for obtained SNPs ($H^+$ stands for HCl treated samples).

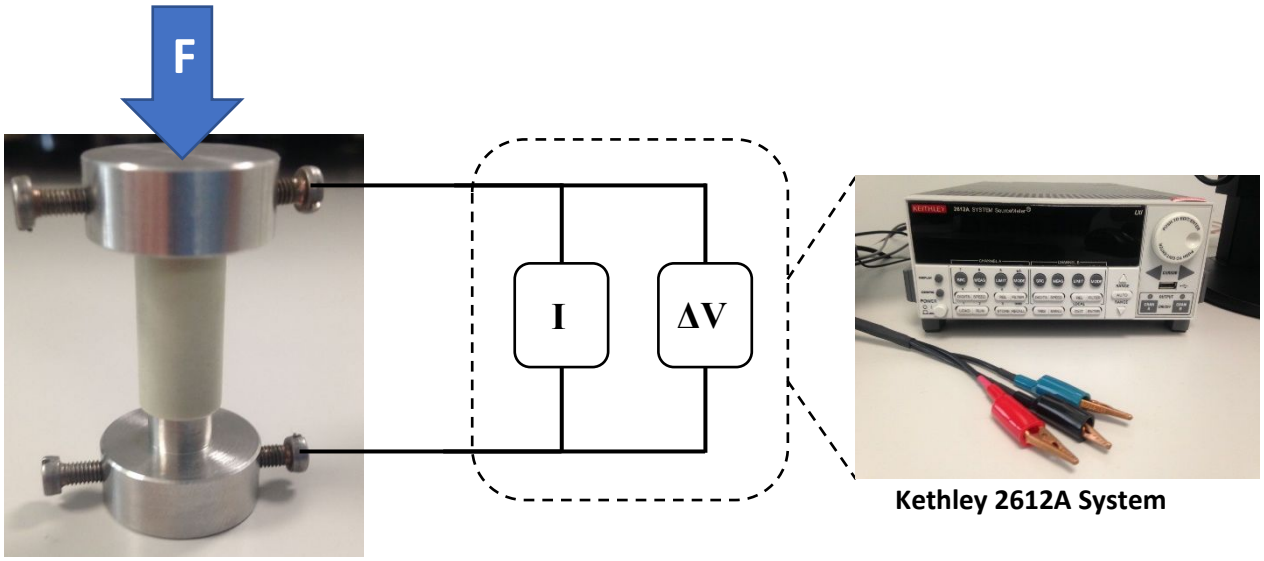


***Figure S46.*** Electronic conductivity measurement setup.

**Electron paramagnetic resonance (EPR) study.**

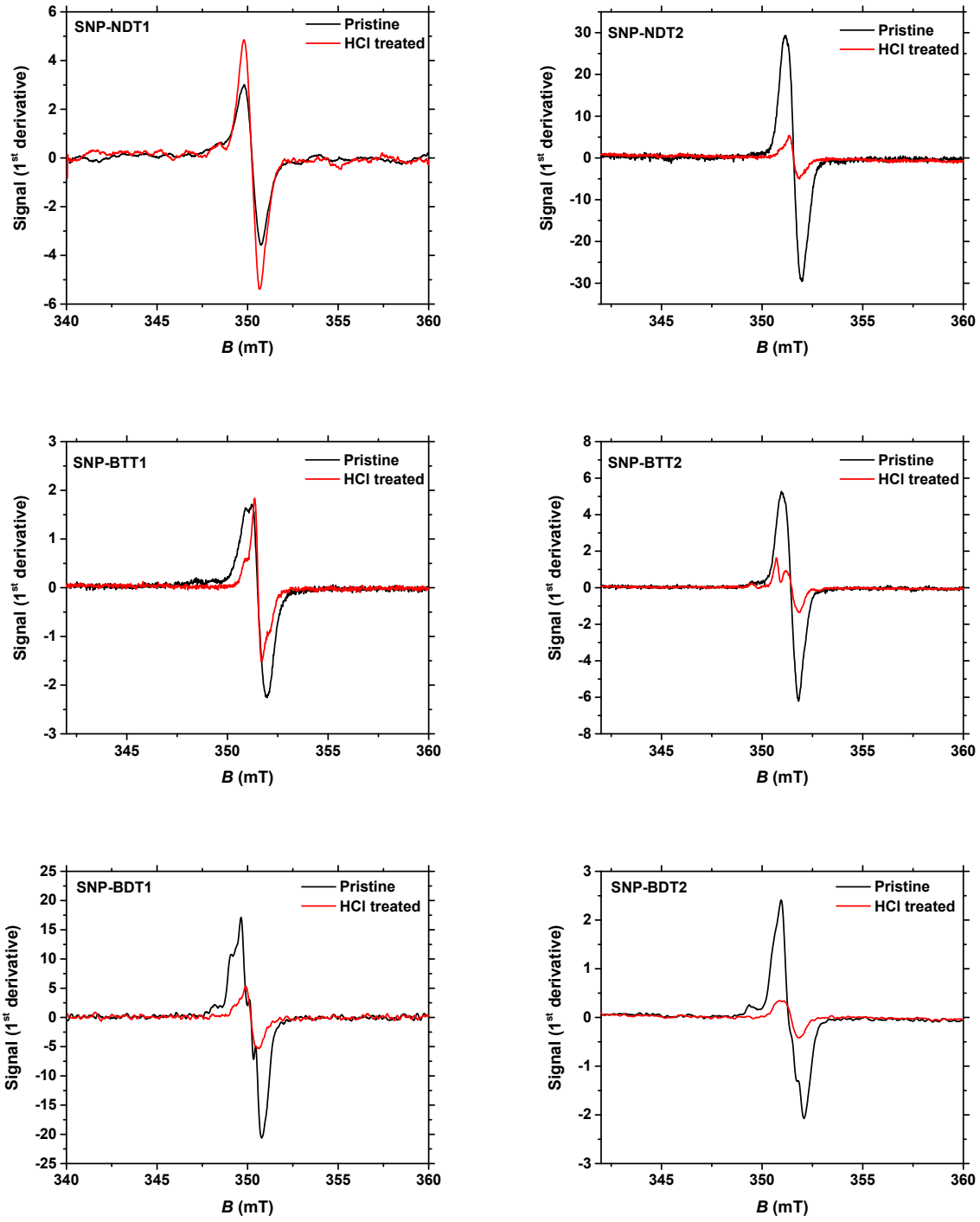


***Figure S47.*** EPR spectra of pristine (black) and HCl treated (red) polymers.

***Table S12.*** Values for g-centre, linewidth and intensity obtained from EPR spectra for prepared materials.

| Polymer | g-centre | Linewidth (mT) | Intensity (max + min; $mg^{-1}$) |
|---|---|---|---|
| **SNP-NDT1** | 2.0037 | 0.67 | 9.9 |
| **SNP-NDT1 HCl** | 2.0041 | 0.48 | 15.3 |
| **SNP-NDT2** | 2.0037 | 0.83 | 59.0 |
| **SNP-NDT2 HCl** | 2.0036 | 0.47 | 10.4 |
| **SNP-BTT1** | 2.0035 | 0.78 | 3.9 |
| **SNP-BTT1 HCl** | 2.0038 | 0.36 | 3.4 |
| **SNP-BTT2** | 2.0045 | 0.82 | 11.4 |
| **SNP-BTT2 HCl** | 2.0042 | 1.12 | 3.0 |
| **SNP-BDT1** | 2.0044 | 1.12 | 39.8 |
| **SNP-BDT1 HCl** | 2.0036 | 0.69 | 12.1 |
| **SNP-BDT2** | 2.0043 | 1.14 | 4.6 |
| **SNP-BDT2 HCl** | 2.0045 | 0.82 | 0.8 |
| **SP-BTT** | 2.0041 | 1.26 | 2.4 |
| **SP-BTT HCl** | 2.0034 | 0.46 | 29.2 |

**Additional temperature-dependent EPR study for SNP-NDT1 and SP-BTT networks**

The temperature variable experiments in the region of 303 – 403 K were controlled by a liquid/gas nitrogen unit ER4141VT-U and the Win-EPR acquisition software (both from Bruker). The EPR tube with the powder-sample was stabilized at each temperature step, subsequently the spectrum was recorded, and the next temperature was adjusted. The EPR spectra were acquired for one temperature increase – decrease cycle Simulations of the EPR spectra were performed in MATLAB toolbox EasySpin (v. 5.2.20) by least-squares fitting to an experimental spectrum using a combination of Nelder-Mead simplex and Particle swarm algorithms.[9] Instrumental parameters such as microwave frequency, central field, sweep width, number of points and modulation

amplitude were included in the simulation. For the simulation of paramagnetic/radical centres within the **SP-BTT** polymer one or two equivalent protons were considered to interact with the unpaired electron. The temperature dependence of the *g*-factor and the linewidth ($\Delta B_{pp}$) for both samples are presented in Figure S47 and S48. Due to the anisotropy the EPR linewidth was determined as $\Delta B_{pp}$ of the "global" maximum and minimum, therefore it is denoted as $\Delta B_{pp}{}^{max}$.

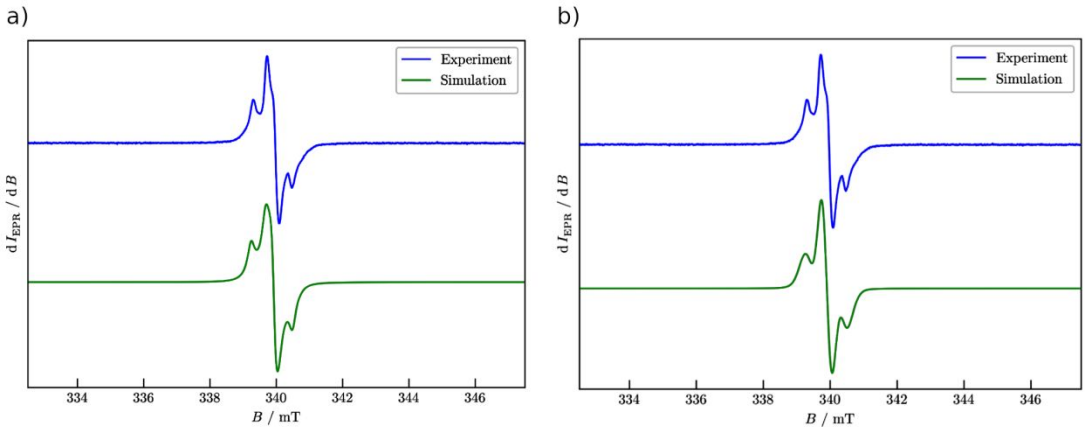


***Figure S48.*** Simulation of the **SP-BTT** EPR spectra considering interaction with a) one or b) two equivalents of protons $^{1}$H.

***Table S13.*** Simulated parameters for radical centre interacting with one two equivalents of protons within the **SP-BTT** framework.

| **Nuclei** | $g_1$ | $g_2$ | $g_3$ | $A_1\,(MHz)$ | $A_2\,(MHz)$ | $A_3\,(MHz)$ |
|---|---|---|---|---|---|---|
| **one equiv. $^{1}$H** | 2.0037 | 2.0068 | 2.0022 | 2.904 | 12.195 | **14.225** |
| **two equiv. $^{1}$H** | **2.0040** | **2.0041** | **2.0044** | **1.150** | **13.550** | **16.568** |

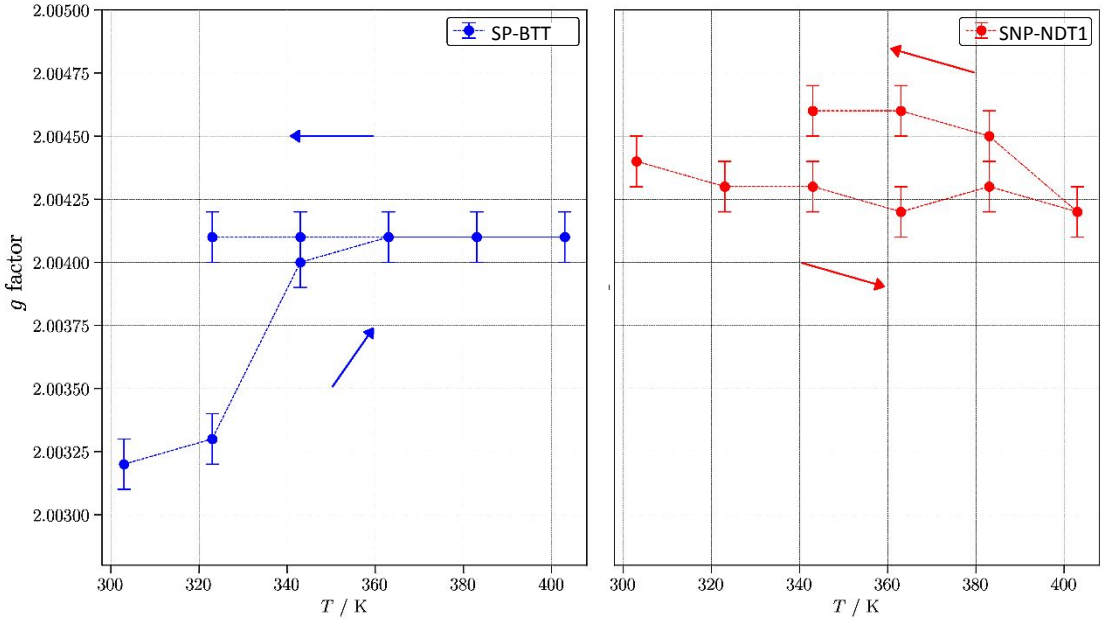


***Figure S49.*** Temperature dependence of the *g*-factor for **SP-BTT** (in blue) and **SNP-NDT1** (in red).

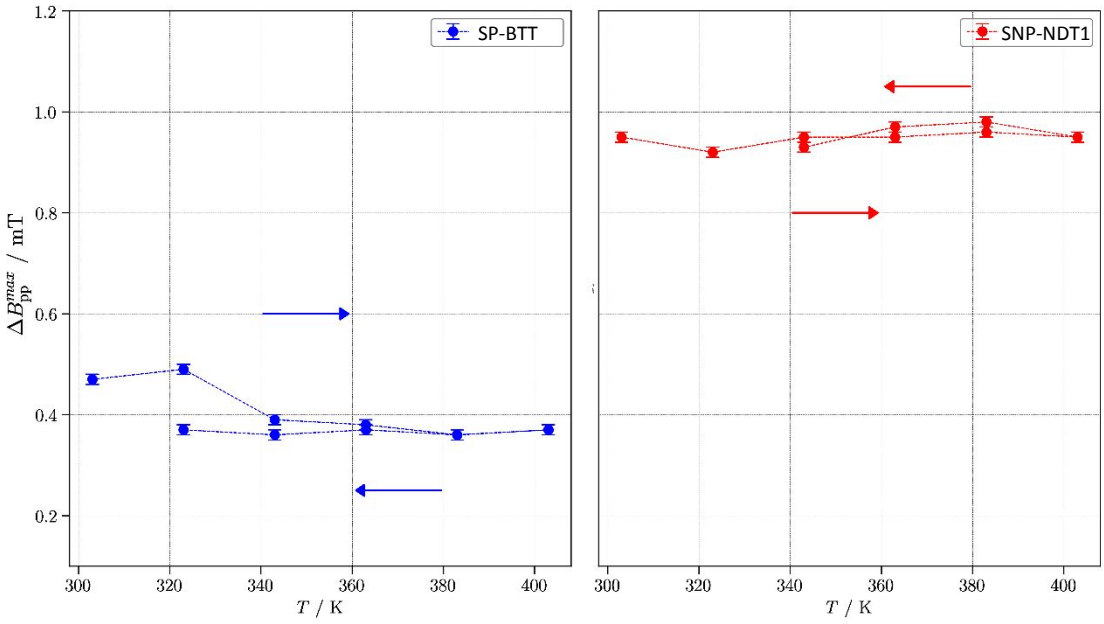


***Figure S50.*** Temperature dependence of the $\Delta B_{pp}^{max}$ for **SP-BTT** (in blue) and **SNP-NDT1** (in red).

## References


1. Tauc, J.; Grigorovici, R.; Vancu, A., Optical Properties and Electronic Structure of Amorphous Germanium. *physica status solidi (b)* **1966,** *15* (2), 627-637.
2. Rungtaweevoranit, B.; Butsuri, A.; Wongma, K.; Sadorn, K.; Neranon, K.; Nerungsi, C.; Thongpanchang, T., A facile two-step synthesis of thiophene end-capped aromatic systems. *Tetrahedron Lett.* **2012,** *53* (14), 1816-1818.
3. Kashiki, T.; Kohara, M.; Osaka, I.; Miyazaki, E.; Takimiya, K., Synthesis and Characterization of Benzo[1,2-b:3,4-b′:5,6-b″]trithiophene (BTT) Oligomers. *J. Org. Chem.* **2011,** *76* (10), 4061-4070.
4. Shi, S.; Xie, X.; Gao, C.; Shi, K.; Chen, S.; Yu, G.; Guo, L.; Li, X.; Wang, H., Synthesis and Characterization of Angular-Shaped Naphtho[1,2-b;5,6-b′]difuran–Diketopyrrolopyrrole-Containing Copolymers for High-Performance Organic Field-Effect Transistors. *Macromolecules* **2014,** *47* (2), 616-625.
5. Morse, G. E.; Tournebize, A.; Rivaton, A.; Chasse, T.; Taviot-Gueho, C.; Blouin, N.; Lozman, O. R.; Tierney, S., The effect of polymer solubilizing side-chains on solar cell stability. *Phys. Chem. Chem. Phys* **2015,** *17* (17), 11884-11897.
6. Ranganathan, A.; Heisen, B. C.; Dix, I.; Meyer, F., A triazine-based three-directional rigid-rod tecton forms a novel 1D channel structure. *Chem. Commun.* **2007,** (35), 3637-3639.
7. Kashiki, T.; Kohara, M.; Osaka, I.; Miyazaki, E.; Takimiya, K., *J. Org. Chem.* **2011,** *76* (10), 4061-4070.
8. Kochergin, Y. S.; Schwarz, D.; Acharjya, A.; Ichangi, A.; Kulkarni, R.; Eliášová, P.; Vacek, J.; Schmidt, J.; Thomas, A.; Bojdys, M. J., Exploring the "Goldilocks Zone" of Semiconducting Polymer Photocatalysts via Donor-Acceptor Interactions. *Angew. Chem. Int. Ed.* **2018,** *57*, 14188–14192.
9. Stoll, S.; Schweiger, A., EasySpin, a comprehensive software package for spectral simulation and analysis in EPR. *J. Magn. Reson.* **2006,** *178* (1), 42-55.